Joint MIMO Precoding and Computation Resource Allocation for Dual-Function Radar and Communication Systems With Mobile Edge Computing

Changfeng Ding, *Graduate Student Member, IEEE*, Jun-Bo Wang, *Member, IEEE*, Hua Zhang, *Member, IEEE*, Min Lin, *Member, IEEE*, and Geoffrey Ye Li, *Fellow, IEEE*

***Abstract*— In this paper, an integrated communication, radar sensing, and mobile-edge computing (CRMEC) architecture is developed, where user terminals (UTs) perform radar sensing and computation offloading simultaneously at the same spectrum by using multiple-input and multiple-output (MIMO) arrays and dual-function radar-communication techniques. We formulate a multi-objective optimization problem to jointly consider the performance of multi-UT MIMO radar beampattern design and computation offloading energy consumption while jointly optimizing individual transmit precoding for radar and communication and computation resource allocation. To address the optimization problem, we first decompose the it into three subproblems and adopt an iterative optimization algorithm. Specifically, quadratic transform based fractional programming methods are used to minimize the offloading energy consumption. The design objective of MIMO radar beampattern is handled by the first-order Taylor expansion. Transmit precoding is designed to optimize radar sensing and computation task offloading. The local and edge computation resource allocation are obtained in closed-form. Numerical results verify the effectiveness of the proposed algorithms. The proposed CRMEC architecture can generate the desired multi-UT MIMO radar beampattern and perform computation offloading simultaneously.**

***Index Terms*— Dual function radar and communication, mobile edge computing, MIMO precoding, radar sensing.**

I. Introduction

OVER the past decades, numerous machines and robots with sensing abilities have been used to save manpowers, handle dangerous works, and improve the quality of our daily life. As can be seen in the forthcoming sixth generation wireless communication systems, many devices are expected to have sensing capabilities, such as WiFi sensing for smart homes [1], radar sensing for autonomous vehicles [2], [3], and object or obstacle detection for robots. The traditional sensing tools include cameras, infrared sensors, and supersonic sensors, etc. Compared with them, radio-based sensing approach is unobtrusive, ubiquitous, and with robust performance against harsh weather and lighting conditions [1], [2]. Hence, radio-based sensing schemes have attracted both civil and military interests. Meanwhile, radio communication is indispensable for sensing-enabled devices to realize control message exchange and data communication. Traditionally, radar sensing and communication are designed separately and use different hardwares and frequency bands. However, as the number of radar sensing enabled internet-of-thing (IoT) devices increases dramatically, spectrum congestion is becoming a serious problem. Many IoT devices are expected to have small size, low cost, and low power consumption. As a result, the convergence of radar sensing and radio communication in the same frequency band has attracted more and more attention [1]–[5].

Generally, there are two mechanisms for joint radar and communication design: coexistence or cooperation of radar and communication (CRC) systems and dual-function radar-communication (DFRC) systems [6]. In CRC, radar and communication systems are separate and independent and spectrum sharing mainly focuses on interference mitigation schemes, such as cognitive radio access, interference alignment approach, and transmit beamforming [7]–[9]. However, the independent radar and communication systems in CRC require centralized control and some information exchange among the two systems, which are with high complexity and hard to implement. On the other hand, DFRC performs radar sensing and communication on shared spectrum and hardware platform and can be implemented with small size, lightweight, and low cost. Therefore, it can be applied into various user terminals (UTs), such as unmanned aerial vehicles, autonomous cars, and even mobile phones in the future. Undoubtedly, DFRC-enabled UTs will be ubiquitous in the future wireless communication networks. Therefore, in this paper, we investigate the transmission scheme to improve

Manuscript received September 20, 2021; revised December 10, 2021; accepted January 14, 2022. Date of publication March 8, 2022; date of current version June 17, 2022. This work was supported in part by the National Key Research and Development Program of China under Grant 2020YFB1807803, in part by the Key International Cooperation Research Project under Grant 61720106003, in part by the Jiangsu Province Basic Research Project under Grant BK20192002, and in part by the Jiangsu Province Science and Technology Project under Grant BE2021031. *(Corresponding author: Jun-Bo Wang.)*

Changfeng Ding, Jun-Bo Wang, and Hua Zhang are with the National Mobile Communications Research Laboratory, Southeast University, Nanjing 211111, China (e-mail: cfding@seu.edu.cn; jbwang@seu.edu.cn; huazhang@seu.edu.cn).

Min Lin is with the College of Telecommunications and Information Engineering, Nanjing University of Posts and Telecommunications, Nanjing 210003, China (e-mail: linmin@njupt.edu.cn).

Geoffrey Ye Li is with the Department of Electrical and Electronic Engineering, Imperial College London, London SW7 2AZ, U.K. (e-mail: geoffrey.li@imperial.ac.uk).

Color versions of one or more figures in this article are available at https://doi.org/10.1109/JSAC.2022.3157389.

Digital Object Identifier 10.1109/JSAC.2022.3157389

spectral efficiency and system performance of DFRC-enabled UTs.

Recently, DFRC techniques have been widely discussed in industry and academic circles [4], [10], [11]. The joint design of multi-user multiple-input and multiple-output (MU-MIMO) communication and MIMO radar has been considered and two deployment options are compared [4]. Signal model, beampattern modulation based information embedding, and waveform design have been discussed for DFRC in [10]. Different from most of the existing works that use communication signals for radar detection, a novel joint transmit beamforming model for a dual-function MIMO radar and communication transmitter has been proposed, where the radar waveforms and communication symbols are independently transmitted by different beams [11]. Multi-beam design and transmit power allocation for massive MIMO have been used to support efficient beamformed communications and radar sensing in DFRC [12], [13]. Compared with communication signal based radar sensing method [4], [5], the joint transmitter can have spatial degrees of freedom and utilize multiple beams towards communication users and radar targets. Thus, high quality communication can be provided while guaranteeing the performance of radar sensing.

Although radar sensing has various applications, the signal processing and data analysis are usually complex and often require huge amount of computing resource. The accuracy of the extracted result has significant impact on the performance of radar sensing. For example, if surveillance radar needs to determine the presence or absence of targets, it should extract the desired information and reject unwanted signals, such as radar echoes caused by ground clutter, radio frequency interference and noise [14]. As a result, more and more intelligent algorithms, such as machine learning and deep learning algorithms, have been proposed for high performance radar signal or data processing [15], [16], which inevitably turns into heavy computation loads for UTs. Fortunately, mobile edge computing (MEC) is promising to relieve the computation burden of UTs by transferring computation task to the edge of a network, such as the base station (BS) [17], [18]. Thus, UT's radar data can be offloaded to the BS for edge computing and the sensing result can be obtained with high accuracy and shorter delay. Accordingly, we study a multi-UT sensing and communication system, where each UT performs radar sensing and communication simultaneously by using DFRC techniques and MEC technology is used to assist the computation of radar data.

Instead of considering a single device with DFRC ability (e.g., a BS) [4], [11], we investigate a multi-UT scenario, where transmit precoding for radar and communication and computation resource allocation are performed jointly for integrated radar sensing, and mobile-edge computing (CRMEC). The main contributions of this paper are listed as below:

- We propose a CRMEC architecture, where multiple UTs can perform radar sensing and communication via the same frequency band simultaneously. Moreover, MEC is introduced to satisfy the computation demand for radar signal processing and data mining. Furthermore, we formulate a multi-objective optimization (MOO) problem by jointly considering UTs' computation offloading energy consumption and radar beampattern design, where MIMO precoding for computation offloading and radar sensing, and computation resource allocation are optimized jointly.
- We adopt an iterative optimization method to solve the MOO problem. First, we use quadratic transform based fractional programming (QTFP) methods with first-order Taylor expansion to solve the precoding problem for computation offloading. For MIMO radar precoding, we use the weighted minimum mean-squared error (WMMSE) method, QTFP and first-order Taylor expansion methods to transform the MIMO radar beampattern design into a convex and differential problem. Then, we use the Lagrangian dual method to obtain the closed-form results of precoding matrix for MIMO radar sensing and edge computation resource allocation.
- We derive a lower bound of local resource allocation in terms of the delay constraint. Then, we achieve the closed-form result for local computation resource allocation.

The rest of the paper is organized as follows. In Section II, the system model is introduced. Section III formulates the MOO problem. The problem of jointly optimizing transmit precoding and computation resource allocation is addressed in Section IV. Simulation results are given in Section V and the paper is concluded in Section VI.

$Notations$: Lower case boldface letters denote vectors while upper case boldface letters denote matrices. The trace of a matrix $\mathbf{A}$ is denoted by $\mathrm{Tr}\,(\mathbf{A})$. The transpose and conjugate-transpose of matrix $\mathbf{A}$ is denoted by $\mathbf{A}^T$ and $\mathbf{A}^H$, respectively. A positive semi-definite matrix $\mathbf{A}$ is denoted as $\mathbf{A} \succeq \mathbf{0}$. $\mathbb{E}[x]$ denotes the expectation of x. We use diag($\mathbf{a}$) to represent an diagonal matrix with its main diagonal elements from $\mathbf{a}$. The symbol, $\odot$, is the Hadamard product, i.e., the element-wise multiplication of two matrices. $\|\cdot\|_F^2$ denotes the square of Frobenius norm. $\|\cdot\|$ denotes Euclidean norm. $\mathbf{I}_d$ denotes the $d \times d$ identity matrix. $\mathbb{C}^{M\times N}$ denotes the complex space of $M \times N$.

II. System Model and Problem Formulation

As shown in Fig. 1(a), we consider a CRMEC system. Each DFRC-enabled UT has wireless communication and radar detection functions at the same time. First, UT's radar can perform multiple sensing, such as object detection, obstacle detection, and collision detection, for robots, unmanned aerial vehicle (UAV), and cars. Meanwhile, the DFRC-enabled UT can also communicate with the BS for exchanging essential information or realizing centralized control. During the process of radar sensing, a large amount of computation intensive radar data will be generated, thus an edge computing server is deployed at the BS for accelerating the process of UTs' radar data and the sensing results can be quickly obtained with higher accuracy. With DFRC, the UT can perform radar sensing and task data offloading simultaneously.

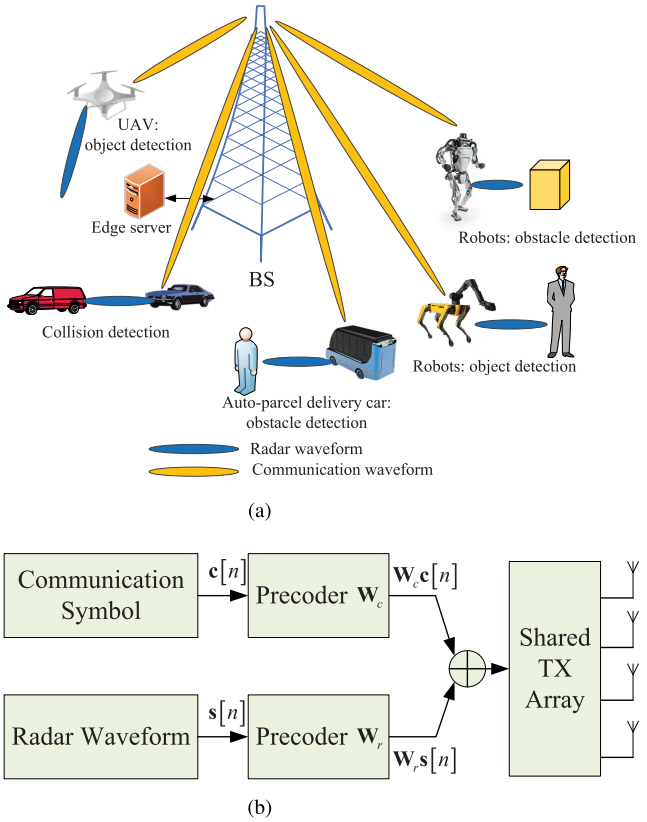

Fig. 1. (a) Integrated design of communication, radar, and mobile edge computing; (b) the joint transmitter jointly precodes both communication symbols and radar waveforms [11].

One of the promising ways to realize the DFRC function is multi-beam based communication and radar shared transmitter as shown in Fig. 1(b), where the transmit signal is the superimposition of individually precoded communication symbols and radar waveforms [11]. Moreover, the radar and communication signals share the same transmit antenna array.

In the CRMEC system, K UTs, denoted as $\mathcal{K} = \{1, 2, \ldots, K\}$, are randomly distributed. Each UT has N antennas and has certain amount of radar data that needs to be processed timely. However, the computation task cannot be executed by the UT alone due to limited computing power and stored energy. The BS equipped an edge server and M antennas can provide computation services for DFRC-enabled UTs.

A. Transmission Signal Model of DFRC-Enabled UT

For the DFRC transmitter in Fig. 1(b), the $N \times 1$ transmit signal vector of UT k at time slot n is given by

$$\mathbf{x}_k[n] = \mathbf{W}_{r,k}\mathbf{s}_k[n] + \mathbf{W}_{c,k}\mathbf{c}_k[n], \tag{1}$$

where the $N \times 1$ vector, $\mathbf{s}_k[n] = [s_{k,1}[n], \cdots, s_{k,N}[n]]^T$, includes N individual radar waveforms, $\mathbf{W}_{r,k} \in \mathbb{C}^{N\times N}$ is the precoding matrix for radar waveforms, $\mathbf{c}_k[n] \in \mathbb{C}^{d\times 1}$ denotes d parallel communication symbols to be transmitted to the BS, and $\mathbf{W}_{c,k} \in \mathbb{C}^{N\times d}$ is the precoding matrix for communication symbols. To facilitate analysis, we have the following assumptions for communication symbol and radar waveform [4], [11]:

TABLE I
SUMMARY OF NOTATIONS

Notation	Definition
$\mathbf{x}_k$	UT k's transmit signal vector
$\mathbf{W}_{r,k}$	UT k's precoding matrix for radar wavefors
$\mathbf{W}_{c,k}$	UT k's precoding matrix for communication symbols
$\mathbf{s}_k$	Radar waveform vector
$\mathbf{c}_k$	Communication symbol vector
$\mathbf{H}_k$	Channel matrix from UT k to BS
$\mathbf{v}$	Additive white gaussian noise vector
α_k	Pathloss between UT k and the radar target
$\mathbf{a}_{T,k}(\theta_k)$	UT k's transmit array steering vector
$\mathbf{a}_{R,k}(\theta_k)$	UT k's receive array steering vector
$\mathbf{R}_{\mathbf{X},k}$	Covariance matrix of UT k's transmit signal
B_k	Generated radar data bits
$E_{l,k}$	UT k's energy consumption of local radar data processing
$T_{l,k}$	UT k's time delay of local radar data processing
r_k	Communication data rate of UT k
$T_{o,k}$	UT k's time delay of task offloading
$E_{o,k}$	UT k's energy consumption of task offloading
$T_{e,k}$	UT k's edge computing time delay
T_k	UT k's overall offloading time delay
$P_{d,k}(\theta_l)$	Desired beampattern gain at angle θ_l of UT k
$\mathbf{R}_{d,k}$	Desired beam pattern of UT k
ρ_k	UT k's average interference-to-noise ratio
ζ_k	The maximum tolerable INR level of UT k
$P_{t,k}$	UT k's transmission power budget
$T_{max,k}$	UT k's maximum delay
$f_{l,k}$	Local computing resource allocated to UT k
$f_{e,k}$	Edge computing resource allocated to UT k
$F_{total,k}$	Total local computing resource of UT k
f_{total}	Total computing resource of edge server

- Radar and communication signals are all zero-mean, temporally-white, and wide-sense stationary stochastic process.
- UTs' communication symbols are uncorrelated with the radar waveforms, i.e., $\mathbb{E}\left(\mathbf{s}_k[n]\,\mathbf{c}_l^H[n]\right) = \mathbb{E}\left(\mathbf{s}_k[n]\right)\mathbb{E}\left(\mathbf{c}_l^H[n]\right) = \mathbf{0}_{N\times d}, \forall k, l \in \mathcal{K}$;
- The communication symbols satisfy $\mathbb{E}\left(\mathbf{c}_k[n]\,\mathbf{c}_k^H[n]\right) = \mathbf{I}_d$ and $\mathbb{E}\left(\mathbf{c}_k[n]\,\mathbf{c}_l^H[n]\right) = \mathbf{0}_d$ for $\forall k \neq l$;
- By using stochastic radar waveform and pseudorandom coding [19], [20], UTs' radar waveforms are uncorrelated and satisfy $\mathbb{E}\left(\mathbf{s}_k[n]\,\mathbf{s}_k^H[n]\right) = \mathbf{I}_N$ and $\mathbb{E}\left(\mathbf{s}_k[n]\,\mathbf{s}_l^H[n]\right) = \mathbf{0}_N$ for $\forall k \neq l$.

Even if the typical deterministic radar waveform cannot satisfy the above requirement, stochastic radar waveform and pseudorandom coding can be applied to generate the desired

radar waveform [19]–[24]. Stochastic radar waveforms here refer to radar waveform coding and modulation, such as BPSK coded waveforms [21], linear frequency modulation of a stochastic radar waveform [22], and stochastic modulation upon amplitude, or frequency, or phase that could increase wavefront variety [24]. Compared with the deterministic radar waveforms, the stochastic radar waveform has advantages of low probability of detection, low probability of interception, and low co-channel interference, etc., [22]. The stochastic waveform is a wide-sense stationary (WSS) process as in [22]. Thus, the assumptions made about communication symbol and radar waveform can be satisfied. The detailed MIMO radar waveform design by using stochastic waveforms is another issue and beyond the scope of our article.

Since each UT's DFRC transmitter transmits precoded individual radar and communication waveforms. The received signal vector at the BS incorporates both communication and radar signals and can be expressed as

$$\begin{aligned}\mathbf{y}^{(c)}[n] &= \sum_{k=1}^{K} \mathbf{H}_k \mathbf{x}_k[n] + \mathbf{v}[n] \\ &= \sum_{k=1}^{K} \mathbf{H}_k (\mathbf{W}_{r,k}\mathbf{s}_k[n] + \mathbf{W}_{c,k}\mathbf{c}_k[n]) + \mathbf{v}[n], \end{aligned} \quad (2)$$

where $\mathbf{H}_k \in \mathbb{C}^{M\times N}$ denotes the communication channel matrix from UT k to the BS and $\mathbf{v}[n]$ is an additive white Gaussian noise (AWGN) vector with covariance $\sigma_c^2\mathbf{I}_M$.

Since UT k uses both the communication signal and the radar waveform for target detection, the covariance of its transmit waveform is denoted by

$$\mathbf{R}_{\mathbf{X},k} = \mathbb{E}\left[\mathbf{x}_k\mathbf{x}_k^H\right] = \mathbf{W}_{r,k}\mathbf{W}_{r,k}^H + \mathbf{W}_{c,k}\mathbf{W}_{c,k}^H. \quad (3)$$

The power constraint for DFRC-enabled UT k is denoted by

$$\mathrm{Tr}\left(\mathbf{R}_{\mathbf{X},k}\right) = \mathrm{Tr}\left(\mathbf{W}_{r,k}\mathbf{W}_{r,k}^H + \mathbf{W}_{c,k}\mathbf{W}_{c,k}^H\right) \le P_{t,k}, \quad (4)$$

where $P_{t,k}$ is the transmit power budget for UT k.

B. Radar Data and Local Computation Model

When performing radar sensing, the UT will generate a large amount of radar data that needs to be processed and analyzed timely. Moreover, the processing of the radar data is usually computation intensive [25]. The reflected radar signal from each receiver is converted into a set of radar data. According to the practical radar engineering practice and radar detection model in [14] and [26], the amount of radar data (in bits) can be modelled as

$$B_k = \hat{\eta}_k \nu_k N_\theta f_s b_k, \quad (5)$$

where $\hat{\eta}_k \ge 1$ is a constant related to the introduced data redundancy, such as tabs and time stamps in the data frame, ν_k is the switching speed of the radar beam, N_θ is the number of quantized angles, f_s is the sampling frequency, and b_k is the number of quantization bits for each sample.

Then, a two-layer computing architecture is adopted for processing the radar data [26], [27]. First, those B_k task bits are preprocessed locally, such as removal of unwanted signals [26] or data compression operation [28]. For example, during radar sensing, the radar receiver continuously monitors the received signal for target detection. However, not all of the received signals are reflected from the target and some are unwanted signals, such as radar echoes caused by ground clutter, radio frequency interference, and noise source, can be cancelled to facilitate the following processing and reduce the data size.

The energy consumption and time delay for local radar data preprocessing are modeled as

$$E_{l,k} = \kappa_{l,k}\alpha_{l,k}B_k f_{l,k}^2, \quad (6)$$

and

$$T_{l,k} = \frac{\alpha_{l,k}B_k}{f_{l,k}}, \quad (7)$$

respectively, where $\kappa_{l,k}$ is a constant related to the hardware architecture of UT k, $\alpha_{l,k}$ (cycles/bit) is the local processing density of UT k, and $f_{l,k}$ (cycles/s) is the allocated local computation resource of UT k [17], [29]. Note that the local computation speed of UT k can be flexibly adjusted via the dynamic voltage scaling technology to satisfy UT's demand [30].

C. Radar Data Computation Offloading Model

When the UT finishes radar data preprocessing, the task bits are offloaded to the BS for further processing and analysis. From equ. (2), the BS can receive each UT's communication signal and radar waveform. Thus, UT's communication signal will be interfered by other UTs' DFRC signal. In addition, UT's radar signal will also bring interference to its communication signal. According to equ. (2), UT k's communication signal received by the BS can be formulated as

$$\begin{aligned}\mathbf{y}_k^{(c)}[n] = &\underbrace{\mathbf{H}_k\mathbf{W}_{c,k}\mathbf{c}_k[n]}_{\substack{\text{Intended communication}\\ \text{signal of UT k}}} + \underbrace{\sum_{i=1}^{K}\mathbf{H}_i\mathbf{W}_{r,i}\mathbf{s}_i[n]}_{\substack{\text{Interference signal from all}\\ \text{UTs' radar signal}}} \\ &+ \underbrace{\sum_{i=1,i\neq k}^{K}\mathbf{H}_i\mathbf{W}_{c,i}\mathbf{c}_i[n]}_{\substack{\text{Interference from inter-UT}\\ \text{communication signal}}} + \mathbf{v}[n]. \end{aligned} \quad (8)$$

Based on the UT k's signal model in equ. (8), the achievable data rate between UT k and the BS is given by

$$r_k = B_w \log\det\left(\mathbf{I}_M + \mathbf{H}_k\mathbf{W}_{c,k}\mathbf{W}_{c,k}^H\mathbf{H}_k^H\mathbf{N}_k^{-1}\right), \quad (9)$$

where B_w is the transmit bandwidth. $\mathbf{N}_k$ is the overall background noise and interference from other UTs, which can be formulated as

$$\begin{aligned}\mathbf{N}_k = &\sum_{i=1}^{K}\mathbf{H}_i\mathbf{W}_{r,i}\mathbf{W}_{r,i}^H\mathbf{H}_i^H \\ &+ \sum_{i=1,i\neq k}^{K}\mathbf{H}_i\mathbf{W}_{c,i}\mathbf{W}_{c,i}^H\mathbf{H}_i^H + \sigma_c^2\mathbf{I}_M. \end{aligned} \quad (10)$$

Accordingly, the offloading time delay and energy consumption for UT k to offload its computation task to the BS can be given by

$$T_{o,k} = \frac{\beta_k B_k}{r_k}, \tag{11}$$

and

$$E_{o,k} = \frac{\beta_k B_k}{r_k} \left\| \mathbf{W}_{c,k} \right\|_F^2, \tag{12}$$

respectively, where $\beta_k > 0$ denotes the ratio of the transmitted data size to the original task data size [31] and $\left\| \mathbf{W}_{c,k} \right\|_F^2$ is UT k's transmit power for computation offloading.

After offloading the computation task to the BS, the computation time delay for executing the task can be expressed as

$$T_{e,k} = \frac{C_k}{f_{e,k}} = \frac{\alpha_{e,k} \beta_k B_k}{f_{e,k}}, \tag{13}$$

where $C_k = \alpha_{e,k} \beta_k B_k$ is the total number of CPU cycles required to accomplish the computation task, $f_{e,k}$ (cycles/s) is the computation resource allocated for UT k, and $\alpha_{e,k}$ (cycles/bit) is the processing density of computation task at edge server.

According to equ. (7), equ. (11), and equ. (13), the overall offloading time delay for UT k is the sum of local computing delay, task transmission delay, and edge computing delay, and can be expressed as

$$T_k = T_{l,k} + T_{o,k} + T_{e,k}. \tag{14}$$

Since the computation result is usually small, the time delay and energy consumption caused by receiving computation result are ignored for simplification as in [29], [32], and [30].

Notably, the performance of communication is coupled with computation offloading and is indicated by the offloading time delay $T_{o,k}$ (equ. (11)) and the transmission energy consumption $E_{o,k}$ (equ. (12)) since high efficiency transmission will lead to shorter data transmission delay and lower transmission energy consumption.

D. Radar Sensing

Due to the structure of joint transmitter, each UT's radar receiver knows exactly the transmitted communication symbols and the communication signals can be also used for radar sensing in the DFRC systems [4], [11]. Therefore, the UT's communication signal is not regarded as interference for its radar receiver [11]. Based on the radar target model [7], [33], if a single point-like target in the far-field is located at direction θ_k for UT k, the received echo by UT k at time index n can be written as

$$\mathbf{y}_k^{(r)}[n] = \alpha_k e^{-jw_D n} \mathbf{A}_k(\theta_k) \mathbf{x}_k[n - n_k] + \sum_{i=1, i \neq k}^{K} \mathbf{H}_{k,i} \mathbf{x}_i[n] + \mathbf{z}_k[n], \tag{15}$$

where $\alpha_k \in \mathbb{C}$ is the complex path loss of the path between UT k's radar and target, $\mathbf{A}_k(\theta_k) = \mathbf{a}_{R,k}(\theta_k) \mathbf{a}_{T,k}^H(\theta_k)$, in which $\mathbf{a}_{T,k}(\theta_k) \in \mathbb{C}^{N \times 1}$ and $\mathbf{a}_{R,k}(\theta_k) \in \mathbb{C}^{N \times 1}$ are transmit and receive array steering vector of UT k's radar, respectively, w_D is the Doppler frequency shift, n_k denotes the sum of propagation delays to and from the target, $\mathbf{H}_{k,i} \in \mathbb{C}^{N \times N}$ is the interference channel matrix from UT i to UT k, and $\mathbf{z}_k[n]$ is the received noise with $\mathbf{z}_k[n] \sim \mathcal{CN}\left(0, \sigma_R^2 \mathbf{I}_N\right)$.

To make the above signal model more tractable, we assume that the pathloss factor, α_k, is identical for all transmit and receive antenna elements since the single point-link target is far-field [33], [34].

Since the radar signal is received from a single point target in the far-field and the Doppler shifts caused by the moving targets are usually assumed to be constant during one radar pulse repetition interval [35], [36], the range-Doppler parameters can be completely compensated [7], [9], [33]. Based on the above assumptions and analysis, equ. (15) can be simplified as

$$\mathbf{y}_k^{(r)}[n] = \alpha_k \mathbf{A}_k(\theta_k) \mathbf{x}_k[n] + \sum_{i=1, i \neq k}^{K} \mathbf{H}_{k,i} \mathbf{x}_i[n] + \mathbf{z}_k[n]. \tag{16}$$

According to the characteristic of DFRC, we have $\mathbf{a}_{T,k}(\theta_k) = \mathbf{a}_{R,k}(\theta_k) = \mathbf{a}_k(\theta_k)$, and the steering vector can be written as

$$\mathbf{a}_k(\theta_k) = \left[1, e^{j\frac{2\pi}{\lambda} d_k \sin(\theta_k)}, \cdots, e^{j\frac{2\pi}{\lambda} d_k (N-1) \sin(\theta_k)}\right]^T \in \mathbb{C}^{N \times 1}, \tag{17}$$

where d_k and λ denote the antenna spacing of UT k and the signal wavelength, respectively. Without loss of generality, we set $d_k = \lambda/2$ for all UTs. Accordingly, the transmit-receive steering matrix $\mathbf{A}_k(\theta_k)$ can be written as $\mathbf{A}_k(\theta_k) = \mathbf{a}_k(\theta_k) \mathbf{a}_k^H(\theta_k)$. For convenience, we omit the time index n in the rest of the paper unless otherwise specified.

Practically, the received radar signal returned from the target will be interfered by the clutter, such as buildings and trees, which can be avoided by no radiating or receiving in the corresponding directions [5] or removed by using the radar signal processing method [14], [26]. Accordingly, we ignore the clutter effect as in [4], [7], [11], [21], [37], and [33]. Therefore, the obtained radar and computation offloading performance can be regarded as an upper bound. A more thorough investigation will be considered as our future work.

The main purpose of MIMO radar beamforming is to direct the transmit beam towards several given directions. According to [38] and [21], the MIMO radar probing signal is designed to match a desired beampattern, which will be discussed in the problem formulation section.

In addition to the MIMO radar beampattern design, the inter-UT signal interference for radar sensing cannot be ignored under multi-UT scenario, which will affect the performance of radar detection. For CRC systems, the average interference-to-noise ratio (INR) [9] or signal-to-interference-plus-noise ratio [7] is adopted as the performance metric for radar detection. Here, we use the average INR as an additional constraint to ensure the received signal quality of

radar sensing. For UT k, its average INR is defined by

$$\rho_k = \frac{\mathbb{E}\left[\sum_{i=1,i\neq k}^{K}\left\|\mathbf{H}_{k,i}\mathbf{x}_i\right\|_F^2\right]}{\mathbb{E}\left[\left\|\mathbf{z}_k\right\|_F^2\right]} = \frac{\sum_{i=1,i\neq k}^{K}\left(\left\|\mathbf{H}_{k,i}\mathbf{W}_{r,i}\right\|_F^2+\left\|\mathbf{H}_{k,i}\mathbf{W}_{c,i}\right\|_F^2\right)}{N\sigma_R^2}. \quad (18)$$

The average INR should be small enough to guarantee the quality of the received radar signal. Hence, proper design is required to ensure the performance of computation offloading while mitigating the inter-UT radar signal interference.

III. Problem Formulation

The proposed CRMEC system includes both radar detection and computation offloading. Therefore, the corresponding performance metrics and constraints should be considered. The precoder of the DFRC based joint transmitter should be designed to facilitate transmit power allocation between radar detection and data communication while mitigating the inter-UT signal interference.

A. Requirement for Radar Sensing

For radar sensing in DFRC system, an important design goal is MIMO radar beampattern [4], [21], [37], [38]. The purpose of radar beampattern design is to have high beampattern gain on the given beam directions, which can be addressed through careful design of the covariance matrix of the sensing signals.

The covariance of transmit waveform, $\mathbf{x}_k$, is $\mathbf{R}_{\mathbf{X},k}$. The design of $\mathbf{R}_{\mathbf{X},k}$ should take the properties of MIMO radar beampattern into consideration, such as main beam directions and desired beampattern gain on different direction. From [4], [21], [37], [38], a constrained least-square problem can be formulated to obtain an desired ideal radar beampattern at the first step, which can be expressed as

$$\begin{aligned}\min_{\eta_k,\mathbf{R}_{d,k}}\ & \sum_{l=1}^{L}\left|\eta_k P_{d,k}\left(\theta_l\right)-\mathbf{a}_k^H\left(\theta_l\right)\mathbf{R}_{d,k}\mathbf{a}_k\left(\theta_l\right)\right|^2\\ s.t.\ & \mathrm{Tr}\left(\mathbf{R}_{d,k}\right)=P_{t,k},\\ & \mathbf{R}_{d,k}\succeq 0,\mathbf{R}_{d,k}=\mathbf{R}_{d,k}{}^H,\\ & \eta_k\geq 0. \end{aligned} \quad (19)$$

where η_k is the scaling factor, $P_{d,k}\left(\theta_l\right)$ is the ideal beampattern gain at angle θ_l, $\{\theta_l\}_{l=1}^{L}$ denotes the angular grids that cover the detection angle range in $[-\pi/2,\pi/2]$, $\mathbf{a}_k\left(\theta_l\right)$ is the steering vector, and $\mathbf{R}_{d,k}$ denotes the desired waveform covariance matrix of UT k.

By solving problem (19), we can obtain a desired covariance matrix $\mathbf{R}_{d,k}$ for $\forall k\in\mathcal{K}$. However, the obtained $\mathbf{R}_{d,k}$ may be not appropriate for the practical system design due to the requirements on offloading delay and radar receiver's average INR, etc. As in [4] and [37], a constrained Frobenius-norm square minimization problem has been formulated to approximate the desired MIMO radar beam pattern for single radar sensing scenario. Motivated by this, the multi-UT radar beampattern approximation problem can be expressed as

$$\begin{aligned}\min_{\mathbb{W}_r,\mathbb{W}_c,\mathbb{F}_l,\mathbb{F}_e}\ & g\left(\mathbb{W}_c,\mathbb{W}_r\right)=\sum_{k=1}^{K}\lambda_k^r\left\|\mathbf{R}_{\mathbf{X},k}-\mathbf{R}_{d,k}\right\|_F^2 && (20)\\ s.t.\ & \mathrm{Tr}\left(\mathbf{R}_{\mathbf{X},k}\right)=P_{t,k},\ \forall k\in\mathcal{K}, && (20a)\\ & \mathbf{R}_{\mathbf{X},k}=\mathbf{R}_{\mathbf{X},k}^H,\ \forall k\in\mathcal{K}, && (20b)\\ & \mathbf{R}_{\mathbf{X},k}\succeq 0,\ \forall k\in\mathcal{K}, && (20c)\\ & T_k\leq T_{\max,k},\quad \forall k\in\mathcal{K}, && (20d)\\ & \sum_{k=1}^{K}f_{e,k}\leq f_{total}, && (20e)\\ & \rho_k\leq\zeta_k,\quad \forall k\in\mathcal{K}, && (20f)\\ & 0<f_{l,k}\leq F_{total,k}. && (20g)\end{aligned}$$

where $\lambda_k^r\in[0,1]$ is the non-negative constant weight for UT k, $T_{\max,k}$ is the maximum tolerable delay of UT k, f_{total} is the total computing resource of the edge server, ζ_k is the maximum tolerable INR level of UT k, and $F_{total,k}$ is the total local computing resource of UT k. $\mathbb{W}_r=\{\mathbf{W}_{r,k}\}_{\forall k\in\mathcal{K}}$, $\mathbb{W}_c=\{\mathbf{W}_{c,k}\}_{\forall k\in\mathcal{K}}$, $\mathbb{F}_l=\{f_{l,k}\}_{\forall k\in\mathcal{K}}$, and $\mathbb{F}_e=\{f_{e,k}\}_{\forall k\in\mathcal{K}}$. Constraints (20a), (20d), (20e), (20f), and (20g) denote the power constraint for the shared deployment of DFRC, the delay constraint for computation offloading, the maximum computing resource constraint at the edge server, the required INR level for UT k, and the local computation resource limit, respectively.

B. Requirement for Computation Offloading

In MEC, energy consumption is an important metric to evaluate the performance of computation offloading. Our aim is to minimize the energy consumption of all UTs during computation offloading. According to equ. (6) and equ. (12), the weighted sum energy consumption minimization problem for computation can be expressed as

$$\begin{aligned}\min_{\mathbb{W}_r,\mathbb{W}_c,\mathbb{F}_l,\mathbb{F}_e}\ & f\left(\mathbb{W}_c,\mathbb{W}_r,\mathbb{F}_l\right)=\sum_{k=1}^{K}\lambda_k^c\left(E_{l,k}+E_{o,k}\right) && (21)\\ s.t.\ & \left\|\mathbf{W}_{r,k}\right\|_F^2+\left\|\mathbf{W}_{c,k}\right\|_F^2\leq P_{t,k},\forall k\in\mathcal{K}, && \\ & (20d)-(20g). && (21a)\end{aligned}$$

where $\lambda_k^c\in[0,1]$ is a non-negative constant weight factor for UT k.

C. Multi-Objective Optimization Problem

MIMO radar often transmits at the maximum available power to improve detection performance, such as range and resolution [38]. If the purpose of computation offloading is to minimize the offloading energy consumption, a lower communication transmit power is preferred. As a result, the objective functions of problem (20) and problem (21) are correlated with each other. Thus, we formulate a MOO problem to address the above issue.

The optimization objectives in (20) and (21) can be combined into the MOO problem by

$$\min_{\mathbb{W}_r,\mathbb{W}_c,\mathbb{F}_l,\mathbb{F}_e}\ \gamma_c f\left(\mathbb{W}_c,\mathbb{W}_r,\mathbb{F}_l\right)+\gamma_r g\left(\mathbb{W}_c,\mathbb{W}_r\right) \quad (22)$$

$$s.t. \quad \|\mathbf{W}_{r,k}\|_F^2 + \|\mathbf{W}_{c,k}\|_F^2 \le P_{t,k}, \forall k \in \mathcal{K}, \\ (20d) - (20g). \tag{22a}$$

In (22), γ_c and γ_r, with $\gamma_c + \gamma_r = 1$, represent the priority of computation offloading and radar beampattern design, respectively. In (22a), the maximum transmit power constraint is also relaxed to allow flexible power allocation.

IV. Algorithm Design

Due to the nonconvex objective function and constraints, it is very hard to obtain a global optimal solution for problem (22). Alternatively, we propose a joint algorithm to obtain a suboptimal solution in iterative manner. We first address MIMO precoding for computation offloading and then design precoding for radar sensing and computation resource allocation for edge server. We finally optimize the local computation resource allocation.

A. Precoding Design for Computation Offloading

In this subsection, we tackle the precoding design for computation data offloading. Given $\mathbb{W}_r$, $\mathbb{F}_l$, and $\mathbb{F}_e$, the precoding optimization subproblem for MEC can be given by

$$\min_{\mathbb{W}_c} \ \gamma_c \sum_{k=1}^{K} \lambda_k^c \frac{\beta_k B_k}{r_k} \|\mathbf{W}_{c,k}\|_F^2 + \gamma_r g(\mathbb{W}_c), \tag{23}$$

subject to constraints (20d), (20f), and (22a). From problem (23), the objective function consists of the energy consumption for data transmission, $f(\mathbb{W}_c)$, and MIMO radar beampattern approximation, $g(\mathbb{W}_c)$. Here, we handle those two objectives in order.

The first part of transmission energy consumption, $f(\mathbb{W}_c)$, is complex and nonconvex due to the fractional terms. Hence, it belongs to the fractional programming problem [39] and can be further identified as a sum-of-ratios problem [40], [41]. The sum-of-ratios can be well addressed by the quadratic transform method [18], [42].

By applying the quadratic transform method to the fractional term, $\|\mathbf{W}_{c,k}\|_F^2 \big/ R_k$, $f(\mathbb{W}_c)$ can be equivalently rewritten as

$$f_q(\mathbb{W}_c, \mathbf{e}) = \sum_{k=1}^{K} \lambda_k^c \beta_k B_k \left(2e_k \sqrt{\|\mathbf{W}_{c,k}\|_F^2} - e_k^2 r_k \right), \tag{24}$$

where $\mathbf{e} = \{e_k \in \mathbb{R} | \forall k \in \mathcal{K}\}$ is the collection of auxiliary variables.

From equ. (24), $\sqrt{\|\mathbf{W}_{c,k}\|_F^2}$ is convex and the offloading time delay $T_{o,k}$ in constraint (20d) is a fractional term with respect to (w.r.t) r_k. Thus, the convexity of $f_q(\mathbb{W}_c, \mathbf{e})$ and constraint (20d) over $\mathbb{W}_c$ can be determined if r_k is recast as a concave function. Since the optimization variables are coupled and also inside the $\log\det()$ function of r_k, it is nonconvex and hard to handle. Using the transformation method used in [18], r_k can be changed into a concave function by using the following methods.

First, let $\mathbf{w}_{c,k(l)}$ be the l-th column of precoding matrix $\mathbf{W}_{c,k}$. Then, r_k can be rewritten as the sum of the rate contributions by different streams received at the BS, which can be expressed as

$$\tilde{r}_k = \sum_{l=1}^{d} B_w \log\left(1 + \mathbf{w}_{c,k(l)}^H \mathbf{H}_k^H \mathbf{N}_k^{-1} \mathbf{H}_k \mathbf{w}_{c,k(l)}\right). \tag{25}$$

Then, the Lagrangian dual transform can be applied to (25) and we have the following theorem, proved in Appendix A.

Theorem 1: (Lagrangian Dual Transform in Multidimensional and Complex Case). By using the Lagrangian dual transform method, the sum of logarithms in (25) can be reformulated as

$$\tilde{r}_k(\mathbb{W}_c, \gamma) = \sum_{l=1}^{d} B_w (1+\gamma_{k,l}) \mathbf{w}_{c,k(l)}^H \mathbf{H}_k^H \mathbf{U}_{k,l}^{-1} \mathbf{H}_k \mathbf{w}_{c,k(l)} + s(\gamma), \tag{26}$$

where $\gamma = \{\gamma_{k,l} | \forall k \in \mathcal{K}, l = 1, \ldots, d\}$ is the collection of auxiliary variables, $\mathbf{U}_{k,l} = \mathbf{H}_k \mathbf{w}_{c,k(l)} \mathbf{w}_{c,k(l)}^H \mathbf{H}_k^H + \mathbf{N}_k$, and $s(\gamma) = \sum_{l=1}^{d} B_w (log(1+\gamma_{k,l}) - \gamma_{k,l})$ is a constant when γ is fixed.

For a given $\mathbf{w}_{c,k(l)}$, the optimal $\gamma_{k,l}$ can be obtained by setting $\partial \tilde{r}_k(\mathbf{W}_c, \gamma)/\partial \gamma_{k,l} = 0$, that is,

$$\gamma_{k,l}^{opt} = \mathbf{w}_{c,k(l)}^H \mathbf{H}_k^H \mathbf{N}_k^{-1} \mathbf{H}_k \mathbf{w}_{c,k(l)}. \tag{27}$$

However, after the above transformation, $\tilde{r}_k(\mathbb{W}_c, \gamma)$ is still nonconcave w.r.t $\mathbb{W}_c$ due to the coupled variables of $\mathbf{w}_{c,k(l)}^H \mathbf{H}_k^H \mathbf{U}_{k,l}^{-1} \mathbf{H}_k \mathbf{w}_{c,k(l)}$. Following [42], by applying multidimensional quadratic transform method to $\tilde{r}_k(\mathbb{W}_c, \gamma)$, $\tilde{r}_k(\mathbb{W}_c, \gamma)$ can be further recast as

$$\tilde{r}_k(\mathbb{W}_c, \gamma, \mathbb{Z}) = \sum_{l=1}^{d} 2\sqrt{B_w(1+\gamma_{k,l})} \mathrm{Re}\left\{\mathbf{w}_{c,k(l)}^H \mathbf{H}_k^H \mathbf{z}_{k,l}\right\} - \sum_{l=1}^{d} \mathbf{z}_{k,l}^H \mathbf{U}_{k,l} \mathbf{z}_{k,l} + s(\gamma), \tag{28}$$

where $\mathbf{z}_{k,l} \in \mathbb{C}^{M \times 1}$ is an auxiliary vector and $\mathbb{Z} = \{\mathbf{z}_{k,l} | \forall k \in \mathcal{K}, \}$.

Moreover, by taking the expression of $\mathbf{U}_{k,l}$ into equ. (28), $\tilde{r}_k(\mathbb{W}_c, \gamma, \mathbb{Z})$ can be reformulated as

$$\begin{aligned} \tilde{r}_k(\mathbb{W}_c, \gamma, \mathbb{Z}) = & \sum_{l=1}^{d} 2\sqrt{B_w(1+\gamma_{k,l})} \mathrm{Re}\left\{\mathbf{w}_{c,k(l)}^H \mathbf{H}_k^H \mathbf{z}_{k,l}\right\} \\ & + s(\gamma) - \sum_{l=1}^{d} \left\|\mathbf{z}_{k,l}^H \mathbf{H}_k \mathbf{w}_{c,k(l)}\right\|_F^2 \\ & - \sigma_c^2 \sum_{l=1}^{d} \|\mathbf{z}_{k,l}\|_F^2 - \sum_{l=1}^{d} \sum_{i=1}^{K} \left\|\mathbf{z}_{k,l}^H \mathbf{H}_i \mathbf{W}_{r,i}\right\|_F^2 \\ & - \sum_{l=1}^{d} \sum_{i=1, i \ne k}^{K} \left\|\mathbf{z}_{k,l}^H \mathbf{H}_i \mathbf{W}_{c,i}\right\|_F^2. \end{aligned} \tag{29}$$

From equ. (29), $\sqrt{B_w(1+\gamma_{k,l})}$ and $s(\gamma)$ are both concave over γ. The term $\mathrm{Re}\left\{\mathbf{w}_{c,k(l)}^H \mathbf{H}_k^H z_{k,l}\right\}$ is affine w.r.t $\mathbb{W}_c$ and $\mathbb{Z}$, respectively. While the last three terms in equ. (29) are concave w.r.t $\mathbb{W}_c$ and $\mathbb{Z}$ because the square of Frobenius-norm

is convex. Finally, $\tilde{r}_k\left(\mathbb{W}_c,\gamma,\mathbb{Z}\right)$ is concave w.r.t $\mathbb{W}_c$, γ, and $\mathbb{Z}$, respectively.

On the other hand, $g\left(\mathbb{W}_c\right)$ is nonconvex over $\mathbb{W}_c$ due to the coupled variables inside the square of Frobenius-norm, which can be handled via the first-order Taylor expansion. For simplicity, let $g_c\left(\mathbf{W}_{c,k}\right)=\left\|\mathbf{W}_{c,k}\mathbf{W}_{c,k}^H+\mathbf{W}_{r,k}\mathbf{W}_{r,k}^H-\mathbf{R}_{d,k}\right\|_F^2$. Then, the first-order Taylor expansion of $g_c\left(\mathbf{W}_{c,k}\right)$ around a feasible solution set $\mathbb{W}_c^n$ can be written as

$$\begin{aligned} &g_c\left(\mathbf{W}_{c,k},\mathbf{W}_{c,k}^n\right)\\ &\quad=g_c\left(\mathbf{W}_{c,k}^n\right)\\ &\qquad+\mathrm{Re}\left\{\mathrm{Tr}\left(\left(\nabla g_c\left(\mathbf{W}_{c,k}^n\right)\right)^H\left(\mathbf{W}_{c,k}-\mathbf{W}_{c,k}^n\right)\right)\right\}, \end{aligned} \tag{30}$$

where

$$\begin{aligned} \nabla g_c\left(\mathbf{W}_{c,k}^n\right)&=\frac{\partial g_c\left(\mathbf{W}_{c,k}\right)}{\partial \mathbf{W}_{c,k}}\Big|_{\mathbf{W}_{c,k}=\mathbf{W}_{c,k}^n}\\ &=4\left(\mathbf{W}_{c,k}^n\left(\mathbf{W}_{c,k}^n\right)^H+\mathbf{W}_{r,k}\mathbf{W}_{r,k}^H-\mathbf{R}_{d,k}\right)\mathbf{W}_{c,k}^n. \end{aligned} \tag{31}$$

Following equ. (30) and equ. (31), at the n-th iteration, $g\left(\mathbb{W}_c\right)$ can be denoted by

$$g\left(\mathbb{W}_c,\mathbb{W}_c^n\right)=\sum_{k=1}^{K}\lambda_k^r g_c\left(\mathbf{W}_{c,k},\mathbf{W}_{c,k}^n\right). \tag{32}$$

Obviously, $g\left(\mathbb{W}_c,\mathbb{W}_c^n\right)$ is convex w.r.t $\mathbb{W}_c$.

According to equ. (29) and equ. (31), problem (23) can be reformulated as

$$\begin{aligned} \min_{\mathbb{W}_c,\mathbf{e},\gamma,\mathbb{Z}}\ &\gamma_c\sum_{k=1}^{K}\lambda_k^c\beta_k B_k\left(2e_k\sqrt{\left\|\mathbf{W}_{c,k}\right\|_F^2}-e_k^2\tilde{r}_k\left(\mathbb{W}_c,\gamma,\mathbb{Z}\right)\right)\\ &+\gamma_r g\left(\mathbb{W}_c,\mathbb{W}_c^n\right), \end{aligned} \tag{33}$$

$$s.t.\quad \left\|\mathbf{W}_{c,k}\right\|_F^2+\left\|\mathbf{W}_{r,k}\right\|_F^2\le P_{t,k},\quad \forall k\in\mathcal{K}, \tag{33a}$$

$$\frac{\beta_k B_k}{T_{\max,k}-\frac{\alpha_{l,k}B_k}{f_{l,k}}-\frac{\alpha_{e,k}\beta_k B_k}{f_{e,k}}}-\tilde{r}_k\left(\mathbb{W}_c,\gamma,\mathbb{Z}\right)\le 0,\quad (20e),\ (20f). \tag{33b}$$

where constraint (33b) is derived from constraint (20d).

Problem (33) is now convex w.r.t $\mathbb{W}_c$ and the optimal solution can be found by using a numerical method. Therefore, we propose an interior point method based iterative optimization algorithm to solve problem (33). For the auxiliary variables introduced in the above analysis, when other variables are fixed, the optimal e_k and $\mathbf{z}_{k,l}$ can be given by

$$e_k^{opt}=\frac{\sqrt{\left\|\mathbf{W}_{c,k}\right\|_F^2}}{r_k(\mathbb{W}_c)}, \tag{34}$$

and

$$\mathbf{z}_{k,l}^{opt}=\mathbf{U}_{k,l}^{-1}\sqrt{B_w\left(1+\gamma_{k,l}\right)}\mathbf{H}_k\mathbf{w}_{c,k(l)}, \tag{35}$$

respectively.

For fixed $\mathbf{e}$, γ, and $\mathbf{z}$, the optimal solution of $\mathbb{W}_c$ can be obtained by solving problem (33), which is summarized in Algorithm 1.

Algorithm 1 Transmit Precoding Design for Computation Offloading

1: **Initialization**
Given $\mathbb{W}_r$, $\mathbb{F}_l$, and $\mathbb{F}_e$, initialize $\mathbb{W}_c^{(0)}$ into feasible values. Set $n=0$ and maximum number of iterations: N_{max}.
2: **repeat**
3: Given $\mathbb{W}_c^{(n)}$, update $\gamma_{k,l}$, e_k, and $\mathbf{z}_{k,l}$, by equ. (27), equ. (34), and equ. (35), respectively.
4: Update $g\left(\mathbb{W}_c,\mathbb{W}_c^n\right)$ by equ. (32).
5: Obtain $\mathbb{W}_c^{(n+1)}$ by solving problem (33) using interior point method.
6: Set $n=n+1$.
7: **Until**: the objective (33) converges or $n=N_{max}$ and output the optimal solution $\mathbb{W}_c^{(n)}$.

B. Precoding Design for Radar Sensing and Edge Computation Resource Allocation

The radar transmit precoding design and edge computation resource allocation subproblem with fixed $\mathbb{W}_c$ and $\mathbb{F}_l$ can be formulated as

$$\min_{\mathbb{W}_r,\mathbb{F}_e}\ \gamma_c\sum_{k=1}^{K}\lambda_k^c\frac{\beta_k B_k}{r_k}\left\|\mathbf{W}_{c,k}\right\|_F^2+\gamma_r g\left(\mathbb{W}_r\right), \tag{36}$$

subject to constraints (20d), (20e), (20f), and (22a).

Similar to problem (23), the first part of transmission energy consumption in objective (36) also belongs to the sum-of-ratios problem and the quadratic transform method can be used to handle the fractional terms. Accordingly, problem (36) can be transform into the following,

$$\min_{\mathbb{W}_r,\mathbb{F}_e,\mathbf{t}}\ \gamma_c f_q\left(\mathbb{W}_r,\mathbf{t}\right)+\gamma_r g\left(\mathbb{W}_r\right), \tag{37}$$

$$s.t.\quad \frac{\beta_k B_k}{T_{\max,k}-\frac{\alpha_{l,k}B_k}{f_{l,k}}-\frac{\alpha_{e,k}\beta_k B_k}{f_{e,k}}}-r_k\left(\mathbb{W}_r\right)\le 0,\quad \forall k\in\mathcal{K}, \tag{37a}$$

and constraints (20e), (20f), and (22a), where $\mathbf{t}=\{t_k|\forall k\in\mathcal{K}\}$ is the collection of auxiliary variables and $f_q\left(\mathbb{W}_r,\mathbf{t}\right)$ is formulated as

$$f_q\left(\mathbb{W}_r,\mathbf{t}\right)=\sum_{k=1}^{K}\lambda_k^c\beta_k B_k\left\|\mathbf{W}_{c,k}\right\|_F^2\left(2t_k-t_k^2 r_k\left(\mathbb{W}_r\right)\right). \tag{38}$$

When other variables are fixed, the optimal t_k is given by

$$t_k^{opt}=\frac{1}{r_k}. \tag{39}$$

By observing $f_q\left(\mathbb{W}_r,\mathbf{t}\right)$ in (38) and constraint (37a), $f_q\left(\mathbb{W}_r,\mathbf{t}\right)$ and constraint (37a) are convex if $r_k\left(\mathbb{W}_r\right)$ is a concave function.

In the previous section, we use Lagrangian dual transform and multidimensional quadratic transform to recast $r_k\left(\mathbb{W}_c\right)$ as a concave function. However, the iterative optimization process has high complexity.

By using the WMMSE receiver, the estimated signal vector of UT k at the BS can be given as

$$\hat{\mathbf{c}}_k=\mathbf{V}_k^H\mathbf{y}_k^{(c)},\quad \forall k\in\mathcal{K}, \tag{40}$$

where $\mathbf{V}_k \in \mathbb{C}^{M\times d}$ is the receive precoding matrix for UT k. Furthermore, the mean-squared error (MSE) matrix of UT k can be formulated as

$$\begin{aligned}\mathbf{E}_k &= \mathbb{E}_{\mathbf{x},\mathbf{n}}\left[\left(\hat{\mathbf{c}}_k-\mathbf{c}_k\right)\left(\hat{\mathbf{c}}_k-\mathbf{c}_k\right)^H\right]\\ &= \left(\mathbf{V}_k^H\mathbf{H}_k\mathbf{W}_{c,k}-\mathbf{I}_d\right)\left(\mathbf{V}_k^H\mathbf{H}_k\mathbf{W}_{c,k}-\mathbf{I}_d\right)^H\\ &\quad+\sum_{i=1,i\neq k}^{K}\mathbf{V}_k^H\mathbf{H}_i\mathbf{W}_{c,i}\mathbf{W}_{c,i}^H\mathbf{H}_i^H\mathbf{V}_k\\ &\quad+\sum_{i=1}^{K}\mathbf{V}_k^H\mathbf{H}_i\mathbf{W}_{r,i}\mathbf{W}_{r,i}^H\mathbf{H}_i^H\mathbf{V}_k+\sigma_c^2\mathbf{V}_k^H\mathbf{V}_k. \quad (41)\end{aligned}$$

By using $\mathbf{E}_k$ and introducing the auxiliary matrix $\mathbf{G}_k$, the following theorem establishes the relationship between r_k and $\tilde{r}_k\left(\mathbf{G}_k,\mathbb{W}_r,\mathbf{V}_k\right)$, whose details are proved in Appendix B.

Theorem 2: Let $\left\{\mathbf{G}_k\succeq 0\,|\forall k\in\mathcal{K}\right\}$ be a set of auxiliary matrices, the rate function of $r_k\left(\mathbb{W}_r\right)$ can be equivalently reformulated as

$$\tilde{r}_k\left(\mathbf{G}_k,\mathbb{W}_r,\mathbf{V}_k\right)=\log\det\left(\mathbf{G}_k\right)-\mathrm{Tr}\left(\mathbf{G}_k\mathbf{E}_k\right)+d. \quad (42)$$

According to Theorem 2, we can have the following lemma.

Lemma 1: $\tilde{r}_k\left(\mathbf{G}_k,\mathbb{W}_r,\mathbf{V}_k\right)$ is concave for each set of matrices $\mathbf{G}_k$, $\mathbb{W}_r$, and $\mathbf{V}_k$ when the other two are given [43]. The optimal $\mathbf{V}_k$, $\mathbf{G}_k$, and $\mathbf{E}_k$ for $\tilde{r}_k\left(\mathbf{G}_k,\mathbb{W}_r,\mathbf{V}_k\right)$ to achieve the data rate are given respectively by

$$\mathbf{V}_k^{opt}=\mathbf{\Pi}^{-1}\mathbf{H}_k\mathbf{W}_{c,k}, \quad (43)$$

$$\mathbf{G}_k^{opt}=\left(\mathbf{E}_k^{opt}\right)^{-1}, \quad (44)$$

and

$$\mathbf{E}_k^{opt}=\mathbf{I}_d-\mathbf{W}_{c,k}^H\mathbf{H}_k^H\mathbf{\Pi}^{-1}\mathbf{H}_k\mathbf{W}_{c,k}, \quad (45)$$

where $\mathbf{\Pi}$ is expressed as

$$\mathbf{\Pi}=\sum_{i=1}^{K}\mathbf{H}_i\mathbf{W}_{c,i}\mathbf{W}_{c,i}^H\mathbf{H}_i^H+\sum_{i=1}^{K}\mathbf{H}_i\mathbf{W}_{r,i}\mathbf{W}_{r,i}^H\mathbf{H}_i^H+\sigma_c^2\mathbf{I}_M. \quad (46)$$

For equ. (45), $\mathbf{E}_k^{opt}$ is achieved by taking $\mathbf{V}_k^{opt}$ into equ. (41).

Proof: By taking the MSE matrix (41) into equ. (42), we can derive

$$\begin{aligned}&\tilde{r}_k\left(\mathbf{G}_k,\mathbb{W}_r,\mathbf{V}_k\right)\\ &=\log\det\left(\mathbf{G}_k\right)-\sigma_c^2\mathrm{Tr}\left(\mathbf{V}_k^H\mathbf{V}_k\mathbf{G}_k\right)+d\\ &\quad-\mathrm{Tr}\left(\left(\mathbf{V}_k^H\mathbf{H}_k\mathbf{W}_{c,k}-\mathbf{I}_d\right)\mathbf{G}_k\left(\mathbf{V}_k^H\mathbf{H}_k\mathbf{W}_{c,k}-\mathbf{I}_d\right)^H\right)\\ &\quad-\sum_{i=1,i\neq k}^{K}\mathrm{Tr}\left(\mathbf{V}_k^H\mathbf{H}_i\mathbf{W}_{c,i}\mathbf{G}_k\mathbf{W}_{c,i}^H\mathbf{H}_i^H\mathbf{V}_k\right)\\ &\quad-\sum_{i=1}^{K}\mathrm{Tr}\left(\mathbf{V}_k^H\mathbf{H}_i\mathbf{W}_{r,i}\mathbf{G}_k\mathbf{W}_{r,i}^H\mathbf{H}_i^H\mathbf{V}_k\right). \quad (47)\end{aligned}$$

Since the trace function is convex, $\tilde{r}_k\left(\mathbf{G}_k,\mathbb{W}_r,\mathbf{V}_k\right)$ is concave for each variable when others are fixed. ■

With the concave function $\tilde{r}_k\left(\mathbf{G}_k,\mathbb{W}_r,\mathbf{V}_k\right)$, $f_q\left(\mathbb{W}_r,\mathbf{t}\right)$ in (38) and constraint (37a) are both convex. Now, the convexity of problem (37) is determined by $g\left(\mathbb{W}_r\right)$. According to the analysis in the previous section, the first-order Taylor expansion is used here again. First, denote

$$g_r\left(\mathbf{W}_{r,k}\right)=\left\|\mathbf{W}_{r,k}\mathbf{W}_{r,k}^H+\mathbf{W}_{c,k}\mathbf{W}_{c,k}^H-\mathbf{R}_{d,k}\right\|_F^2. \quad (48)$$

Then, the first-order Taylor expansion of $g_r\left(\mathbf{W}_{r,k}\right)$ around a feasible solution set $\mathbb{W}_r^n$ can be written as

$$\begin{aligned}\left(\mathbf{W}_{r,k},\mathbf{W}_{r,k}^n\right)&=g_r\left(\mathbf{W}_{r,k}^n\right)\\ &\quad+\mathrm{Re}\left\{\mathrm{Tr}\left(\left(\nabla g_r\left(\mathbf{W}_{r,k}^n\right)\right)^H\left(\mathbf{W}_{r,k}-\mathbf{W}_{r,k}^n\right)\right)\right\}, \quad (49)\end{aligned}$$

where

$$\nabla g_r\left(\mathbf{W}_{r,k}^n\right)=4\left(\mathbf{W}_{r,k}^n\left(\mathbf{W}_{r,k}^n\right)^H+\mathbf{W}_{c,k}\mathbf{W}_{c,k}^H-\mathbf{R}_{d,k}\right)\mathbf{W}_{r,k}^n. \quad (50)$$

Accordingly, at the n-th iteration, $g\left(\mathbb{W}_r\right)$ can be formulated as

$$g\left(\mathbb{W}_r,\mathbb{W}_r^n\right)=\gamma_r\sum_{k=1}^{K}\lambda_k^r g_r\left(\mathbf{W}_{r,k},\mathbf{W}_{r,k}^n\right). \quad (51)$$

Thus, $g\left(\mathbb{W}_r,\mathbb{W}_r^n\right)$ is now convex w.r.t $\mathbb{W}_r$.

According to the results obtained in the above, problem (36) can be finally reformulated as

$$\begin{aligned}\min_{\mathbb{W}_r,\mathbb{F}_e,\mathbf{t}}\ &\gamma_c\sum\nolimits_{k=1}^{K}\lambda_k^c\beta_k B_k\|\mathbf{W}_{c,k}\|_F^2\left(2t_k-t_k^2\tilde{r}_k\right)\\ &+\gamma_r g\left(\mathbb{W}_r,\mathbb{W}_r^n\right), \quad (52)\\ s.t.\ &\frac{\beta_k B_k}{T_{\max,k}-\frac{\alpha_{l,k}B_k}{f_{l,k}}-\frac{\alpha_{e,k}\beta_k B_k}{f_{e,k}}}-\tilde{r}_k\le 0,\quad \forall k\in\mathcal{K}, \quad (52a)\end{aligned}$$

and constraints (20e), (20f), and (22a).

Problem (52) is now convex and Slater's condition is satisfied [44]. Therefore, the duality gap between problem (52) and its dual problem is zero [44]. Therefore, we can solve problem (52) via the Lagrangian dual method. Mathematically, the Lagrangian function of problem (52) is given by

$$\begin{aligned}&L\left(\mathbb{W}_r,\mathbb{F}_e,\mathbf{t},\delta,\mu,\varepsilon\right)\\ &=\lambda_k^c\beta_k B_k\|\mathbf{W}_{c,k}\|_F^2\left(2t_k-t_k^2\tilde{r}_k\right)\\ &\quad+\gamma_r g\left(\mathbb{W}_r,\mathbb{W}_r^n\right)+\sum_{k=1}^{K}\varepsilon_k\left(\rho_k-\zeta_k\right)\\ &\quad+\sum_{k=1}^{K}\delta_k\left(\|\mathbf{W}_{r,k}\|_F^2+\|\mathbf{W}_{c,k}\|_F^2-P_{t,k}\right)\\ &\quad+\sigma\left(\sum_{k=1}^{K}f_{e,k}-f_{total}\right)\\ &\quad+\sum_{k=1}^{K}\mu_k\left(\frac{\beta_k B_k}{T_{\max,k}-\frac{\alpha_{l,k}B_k}{f_{l,k}}-\frac{\alpha_{e,k}\beta_k B_k}{f_{e,k}}}-\tilde{r}_k\right), \quad (53)\end{aligned}$$

where $\varepsilon=\left\{\varepsilon_k\right\}_{k\in\mathcal{K}}\succeq 0$, $\delta=\left\{\delta_k\right\}_{k\in\mathcal{K}}\succeq 0$, $\sigma\ge 0$ and $\mu=\left\{\mu_k\right\}_{k\in\mathcal{K}}\succeq 0$ are the Lagrangian multipliers associated with constraints (20e), (20f), (22a), and (52a), respectively.

Therefore, the dual function is given by

$$\Phi\left(\delta,\mu,\sigma,\varepsilon\right)=\min_{\mathbb{W}_r,\mathbb{F}_e,\mathbf{t}}\ L\left(\mathbb{W}_r,\mathbb{F}_e,\mathbf{t},\delta,\mu,\sigma,\varepsilon\right). \quad (54)$$

Since problem (54) is convex w.r.t $\mathbb{W}_r$, the dual problem of problem (54) is

$$\max_{\delta,\mu,\sigma,\varepsilon} \ \Phi\left(\delta,\mu,\sigma,\varepsilon\right), \tag{55}$$

$$s.t. \ \ \delta_k \geq 0, \ \mu_k \geq 0, \ \sigma \geq 0, \ \varepsilon_k \geq 0, \ \forall k \in \mathcal{K}. \tag{55a}$$

The objective function in (55) is differentiable and the dual problem is convex w.r.t the dual variables. Thus, the sub-gradient projection method or Newton's method can be applied to solve it. Since problem (54) is convex, the optimal solution of $\mathbb{W}_r$ can be obtained by the following theorem, proved in Appendix C.

Theorem 3: For given δ, μ, and ε, the optimal precoding matrix of UT k for radar sensing is given by $\mathbf{W}_{r,k}^{opt}$ as shown in equ. (56), as shown at the bottom of the next page.

Similarly, the optimal edge computation resource allocation for UT k can be obtained by setting $\partial L/\partial f_{e,k} = 0$ and is given by

$$f_{e,k}^{opt} = \left(\alpha_{e,k}\beta_k B_k + \sqrt{\frac{\mu_k \alpha_{e,k}\beta_k B_k}{\sigma}}\right)\left(T_{\max,k} - \frac{\alpha_{l,k}B_k}{f_{l,k}}\right)^{-1}. \tag{57}$$

Since the dual problem (55) is convex, we can use the sub-gradient method to update the Lagrangian multipliers [45]. The updating procedure is shown as follows

$$\delta_k\left(m+1\right) = \left[\delta_k\left(m\right) - \xi_m^{(\delta)}\left(\|\mathbf{W}_{r,k}\|_F^2 + \|\mathbf{W}_{c,k}\|_F^2 - P_{t,k}\right)\right]^+, \tag{58}$$

$$\mu_k\left(m+1\right) = \left[\mu_k\left(m\right) - \xi_m^{(\mu)}\left(\frac{\beta_k B_k}{T_{\max,k} - \frac{\alpha_{l,k}B_k}{f_{l,k}} - \frac{\alpha_{e,k}\beta_k B_k}{f_{e,k}}} - \tilde{r}_k\right)\right]^+, \tag{59}$$

$$\sigma\left(m+1\right) = \left[\sigma\left(m\right) - \xi_m^{(\sigma)}\left(\sum_{k=1}^{K} f_{e,k} - f_{total}\right)\right]^+, \tag{60}$$

and

$$\varepsilon_k\left(m+1\right) = \left[\varepsilon_k\left(m\right) - \xi_m^{(\varepsilon)}\left(\rho_k - \zeta_k\right)\right]^+, \tag{61}$$

where m is the iteration index, $[x]^+ = \max\{0, x\}$, and $\xi_m^{(\cdot)}$ is a dynamically chosen step-size for obtaining the dual variables at the m-th iteration. The dynamic step-size sequence can be chosen according to the typical self-adaptive scheme [45]. By iteratively optimizing t_k, $\mathbf{V}_k$, $\mathbf{G}_k$, $\mathbf{W}_{r,k}$ in equ. (39), equ. (43), equ. (44) and equ. (56), and updating $\{\delta_k\}_{k\in\mathcal{K}}$, $\{\mu_k\}_{k\in\mathcal{K}}$, σ, and $\{\varepsilon_k\}_{k\in\mathcal{K}}$ according to equ. (58)-(61), the optimal solution of problem (37) can be obtained via the dual gradient method with zero duality gap. The overall algorithm to solve problem (36) is summarized in Algorithm 2.

Algorithm 2 Transmit Precoding Design for Radar Sensing

1: **Initialization**
Given $\mathbb{W}_c$ and $\mathbb{F}_l$, initialize a feasible solution set $\mathbb{W}_r^{(0)}$ and $\mathbb{F}_e^{(0)}$. Set $n = 0$ and maximum number of iterations: N_{max}.
2: **repeat**
3: Given $\mathbb{W}_r^{(n)}$, update t_k, $\mathbf{V}_k$, and $\mathbf{G}_k$ by equ. (39), equ. (43), and equ. (44), respectively.
4: With $\mathbb{W}_r^{(n)}$, obtain $g\left(\mathbb{W}_r, \mathbb{W}_r^n\right)$ by equ. (51).
5: Initialize Lagrange multipliers $\{\delta_k(0)\}_{k\in\mathcal{K}}$, $\{\mu_k(0)\}_{k\in\mathcal{K}}$, $\sigma = 0$, $\{\varepsilon_k(0)\}_{k\in\mathcal{K}}$, set $m = 0$ and maximum number of iterations: M_{max}.
6: **repeat**
7: Obtain the optimal radar precoding design $\mathbf{W}_{r,k}^{opt}$ according to equ. (56).
8: Obtain the optimal edge computation resource allocation $f_{e,k}^{opt}$ according to equ. (57).
9: Update Lagrange multipliers $\{\delta_k(m+1)\}_{k\in\mathcal{K}}$, $\{\mu_k(m+1)\}_{k\in\mathcal{K}}$, σ, and $\{\varepsilon_k(m+1)\}_{k\in\mathcal{K}}$ based on equ. (58)-(61).
10: Set $m = m + 1$.
11: **Until** the objective function (52) converges or $m = M_{max}$.
12: Denote the optimal solution of problem (52) by $\mathbb{W}_r^{n+1}$ and $\mathbb{F}_e^{n+1}$.
13: Set $n = n + 1$.
14: **Until**: the objective function (22) converges or $n = N_{max}$ and output the optimal solution $\mathbb{W}_r^{(n)}$ and $\mathbb{F}_e^n$.

C. Local Computation Resource Allocation

For problem (22) with fixed communication precoding matrices $\mathbb{W}_c$, MIMO radar precoding matrices $\mathbb{W}_r$, and edge computation resource allocation $\mathbb{F}_e$, the local computation resource allocation problem can be formulated as

$$\min_{\mathbb{F}_l} \ \gamma_c \sum_{k=1}^{K} \lambda_k^c \kappa_{l,k} \alpha_{l,k} B_k f_{l,k}^2, \tag{62}$$

$$s.t. \ \ f_{l,k}^{\min} \leq f_{l,k} \leq F_{total,k}, \quad \forall k \in \mathcal{K} \tag{62a}$$

where $f_{l,k}^{\min}$ is derived from constraint (20d) and is expressed as

$$f_{l,k}^{\min} = \frac{\alpha_{l,k}B_k}{T_{\max,k} - \beta_k B_k / r_k - \alpha_{e,k}\beta_k B_k / f_{e,k}}. \tag{63}$$

Problem (62) is convex w.r.t $\mathbb{F}_l$. Since the objective function of problem (62) monotonically increases with $\{f_{l,k}\}_{k\in\mathcal{K}}$, problem (62) can be decomposed into K subproblems to decouple the objective function and constraints. Therefore, the optimal $f_{l,k}$ should be taken at its lower bound as

$$f_{l,k}^{opt} = \min\left\{f_{l,k}^{\min}, F_{total,k}\right\}. \tag{64}$$

D. Proposed Iterative Optimization Algorithm and Complexity Analysis

The overall algorithm to solve problem (22) is summarized in Algorithm 3. In Algorithm 3, an ideal MIMO radar beampattern design is first obtained by solving problem (19). Then, Algorithm 3 iteratively optimizes communication precoding matrices, radar precoding matrices, and computation resource

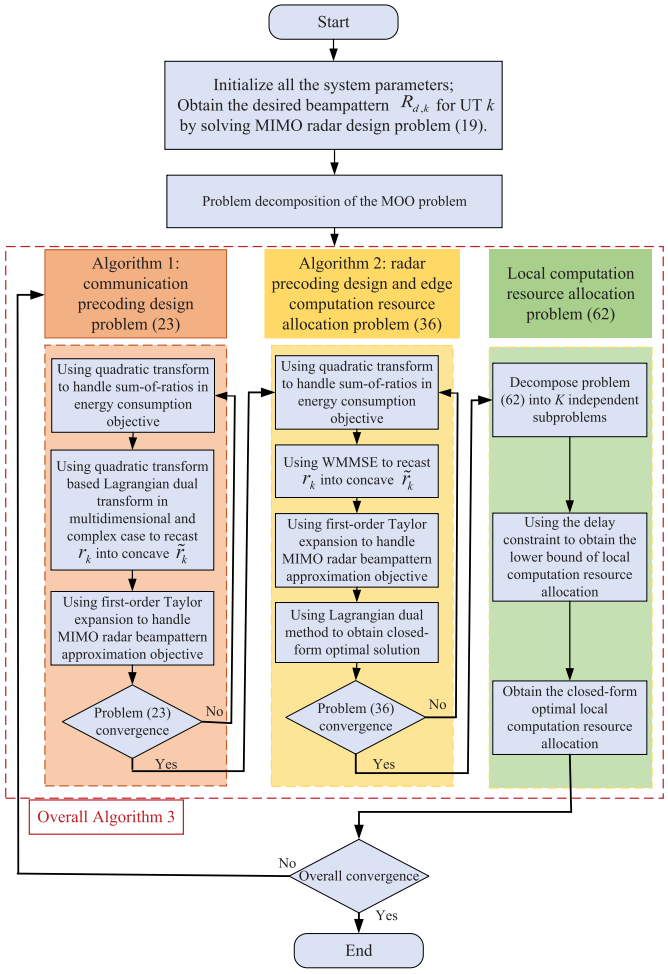

Fig. 2. Block diagram of overall algorithm to solve problem (22).

allocation until the convergence condition is satisfied. The logical flow of those algorithms is shown in Fig. 2.

Theorem 4: The convergence of iterative Algorithm 3 can be ensured.

Proof: See Appendix D. ■

From Algorithm 3, the complexity of each iteration is mainly affected by solving the communication precoding matrix design in Algorithm 1, radar precoding matrix design and edge computation resource allocation in Algorithm 2, and the local computation resource allocation.

The computational complexity of Algorithm 1 mainly comes from Steps 3 to 5 in the loop for L_1 iterations. The complexities of updating auxiliary variables $\gamma_{k,l}$, e_k, and $\mathbf{z}_{k,l}$ in Step 3 are Kd, K, and Kd, respectively. The complexity of updating $g\left(\mathbb{W}_c, \mathbb{W}_c^n\right)$ is K. Since the number of variables to be optimized in Step 5 is KNd, the complexity for solving problem (33) using interior point method is $\mathcal{O}\left(L_1(KNd)^3 + L_1Kd + L_1K\right)$.

The computational complexity of Algorithm 2 comes from the inner loop for L_2 iterations and the outer loop for

Algorithm 3 Iterative Optimization Algorithm for Solving Problem (22)

1: **Initialization**
2: Initialize feasible values of $\mathbb{W}_r^{(0)}$, $\mathbb{W}_c^{(0)}$, $\mathbb{F}_l^{(0)}$ and $\mathbb{F}_e^{(0)}$. Set tolerance $\varepsilon > 0$, $n = 0$ and maximum number of iterations: N_{max}.
3: Obtain MIMO radar beampattern $R_{d,k}$ by solving problem (19).
4: **repeat**
5: Given $\left(\mathbb{W}_r^{(n)}, \mathbb{F}_l^{(n)}, \mathbb{F}_e^{(n)}\right)$, obtain $\mathbb{W}_c^{(n+1)}$ by using Algorithm 1.
6: Given $\left(\mathbb{W}_c^{(n+1)}, \mathbb{F}_l^{(n)}\right)$, obtain $\mathbb{W}_r^{(n+1)}$ and $\mathbb{F}_e^{(n+1)}$ by using Algorithm 2.
7: Given $\left(\mathbb{W}_r^{(n+1)}, \mathbb{W}_c^{(n+1)}, \mathbb{F}_e^{(n+1)}\right)$, obtain $\mathbb{F}_l^{(n+1)}$ according to equ. (64).
8: Set $n = n + 1$.
9: **Until**: the objective function (22) converges or $n = N_{max}$.

L_3 iterations. The complexity of the inner loop for updating the optimization variables and the Lagrangian multipliers are all K. The complexity of the outer loop is also K. Therefore, the total complexity of Algorithm 2 is $\mathcal{O}\left(L_2L_3K^2\right)$. Obviously, the complexity of Step 7 in 3 is K. For Algorithm 3, its overall complexity is shown as $\mathcal{O}\Big(L_0L_1(KNd)^3+L_0L_1Kd+L_0L_1K+L_0L_2L_3K^2+L_0K\Big)$.

V. Simulation and Results

In this section, we present numerical results for the proposed CRMEC system. Assume that the BS and UTs use uniform linear arrays with half-wavelength spaced elements. The number of transmit antennas for UT is $N = 2$ and we set the number of parallel symbols transmitted during each symbol duration as $d = N$. Without loss of generality, the total transmit power, maximum computing capability, and maximum tolerable delay for all UTs are set as $P_{t,k} = P_t = 0.5$W, $F_{total,k} = 0.6$GHz, and $T_{max,k} = T_{max} = 1.5$s, respectively. The number of antennas at the BS is $M = 16$. We adopt the pathloss model as $PL_k\,(\text{dB}) = 148.1 + 37.6\log_{10} l_k(dB)$ [46], and Rayleigh fading with zero mean and unit variance, where l_k (in km) is the distance between UT k and the BS. The total computing power of the BS is set as $f_{total} = 10$GHz. In addition, the local computing density $\alpha_{l.k}$ and edge computing density $\alpha_{e.k}$ are uniformly chosen from $[40.5, 50.5]$ cycles/bit and $[180.5, 283.5]$ cycles/bit, respectively for $\forall k \in \mathcal{K}$, and we set $\kappa_{l,k} = 10^{-25}$ for all UTs. Unless stated otherwise, system parameters are set as follows: $\gamma_c = 0.4$, $\gamma_k^c = 1$, and $\gamma_k^r = 1$ for all UTs. For MIMO radar transmit precoding, the directions of the three main beams are $[-45°, 0°, 45°]$ and the width of each ideal beam is $10°$. $P_{d,k}\,(\theta_l)$ (for all UTs) is set according to [11] and direction angles $\{\theta_l\}_{l=1}^{L}$

$$\mathbf{W}_{r,k}^{opt} = \left[\left(\left[\,\chi_k\mathbf{H}_k^H\mathbf{V}_k\mathbf{V}_k^H\mathbf{H}_k \;\; 2\delta_k\mathbf{I}_N\,\right]\right)^{\dagger}\left(-\gamma_r\gamma_k^r\mathbf{G}_{r,k}\right)\right]_{(N+1):2N,1:N} \tag{56}$$

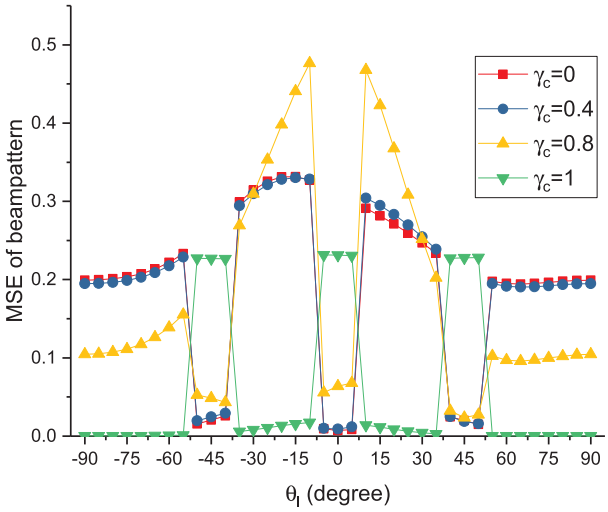

Fig. 3. MSE of beampattern at given direction angle.

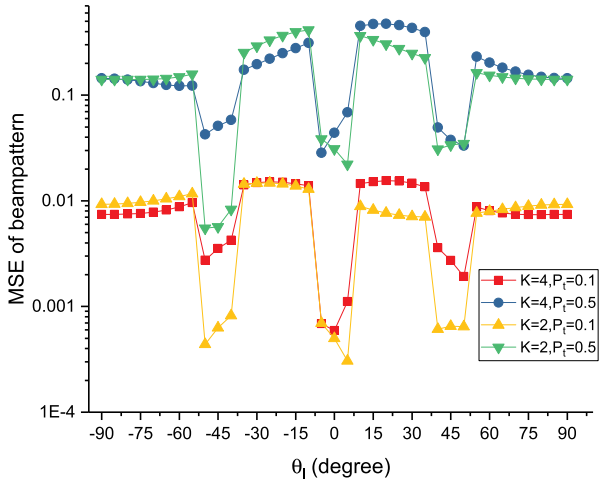

Fig. 4. MSE of beampattern at given direction angle.

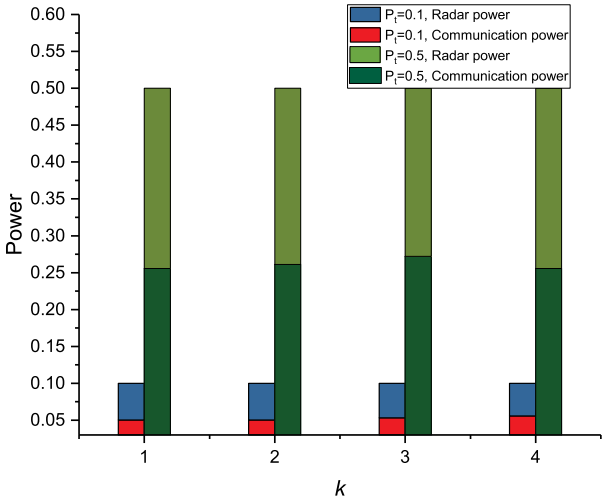

Fig. 5. Power allocation for radar and communication.

are uniformly taken from -90° to 90° with interval of 5°. Hence, the direction angles that fall in the main beam locations are $[-50^\circ, -45^\circ, -40^\circ, -5^\circ, 0^\circ, 5^\circ, 40^\circ, 45^\circ, 50^\circ]$. The average INR requirement is set as $\zeta_k = 0.6$ for all UTs.

First, we evaluate the performance of radar by considering the beampattern of UTs. Since we consider a multi-UT radar sensing scenario, we use the mean-squared error (MSE) of UTs' beampattern versus different direction angles to show radar performance, which is defined as the MSE of UTs' obtained MIMO radar transmit beampattern and the ideal radar-only beampattern at a given direction angle, that is,

$$\mathrm{MSE}(\theta_l)=\frac{1}{K}\sum_{k=1}^{K}\left|\eta_k P_{d,k}\left(\theta_l\right)-\mathbf{a}_k^H\left(\theta_l\right)\mathbf{R}_{\mathbf{X},k}\mathbf{a}_k\left(\theta_l\right)\right|^2, \quad (65)$$

where η_k is the optimal scaling factor obtained by solving radar-only problem (19) and $\mathbf{R}_{\mathbf{X},k}$ is defined as in equ. (3). From equ. (65), a low MSE of beampattern at a given direction angle θ_l indicates the obtained MIMO radar transmit beampattern can approach the ideal radar beampattern very well.

Fig. 3 shows the MSE of beampattern versus the direction angle under different weight coefficients of γ_c. From Fig. 3, the MSE of beampattern for $\gamma_c = 0$, $\gamma_c = 0.4$, and $\gamma_c = 0.8$ is low at the main beam direction angles and adjacent angles while the MSE of beampattern for other angles is high. Therefore, the obtained MIMO radar beampattern has higher beam gain on the desired main beam locations while other directions are suppressed. Moreover, $\gamma_c = 1$ corresponds to the optimization problem in (21), where the radar beampattern design is not considered in the optimization objective. Inevitably, the resultant MSE of beampattern for $\gamma_c = 1$ is dramatically contrary to other MSE of beampattern. When $\gamma_c = 1$, the MSE of beampattern is very high on the main beam locations while the MSE of beampattern on other direction angles is very low. In other words, MIMO radar beampattern design is not considered and has poor performance.

Fig. 4 shows the MSE of beampattern versus the direction angle under different UT numbers and different UT's maximum transmit powers. From Fig. 4, the MSE of beampattern is low on the main beam directions for different values of K and P_t. Moreover, the MSE of beampattern for $P_t = 0.1$ is lower than that of $P_t = 0.5$ because high power budget indicates more power allocation for radar sensing or communication. Taking $K = 4$ as an example, the power allocation for radar and communication under $P_t = 0.1$ and $P_t = 0.5$ is shown in Fig. 5. Since the ideal desired MIMO radar beampattern is designed with full power budget, the power allocation for radar sensing or communication increases with the power budget and the total power approaches the power budget, which will have direct effect on transmit covariance $\mathbf{R}_{\mathbf{X},k}$ as in equ. (3). Hence, the resultant MSE of beampattern increases correspondingly. As the communication signal is also used for radar sensing, the data transmission power for task offloading is affected by the radar function and also increases with the power budget.

Fig. 6 plots the objection function value of the considered MOO problem versus the number of iterations to show the convergence of the proposed algorithms under different UT numbers and transmit power budgets. As can be seen from

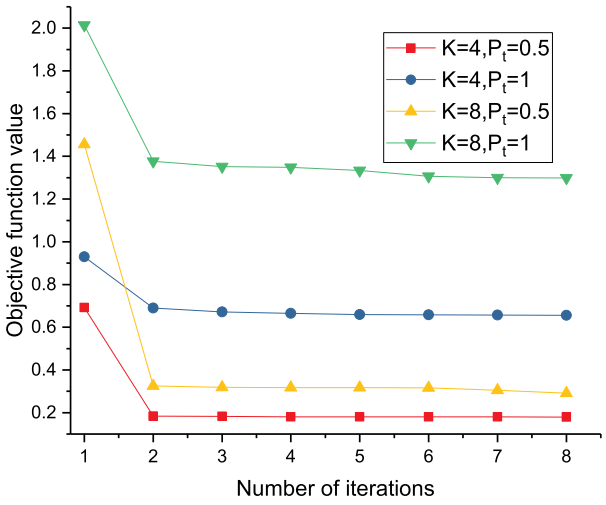

Fig. 6. Convergence of Algorithm 3.

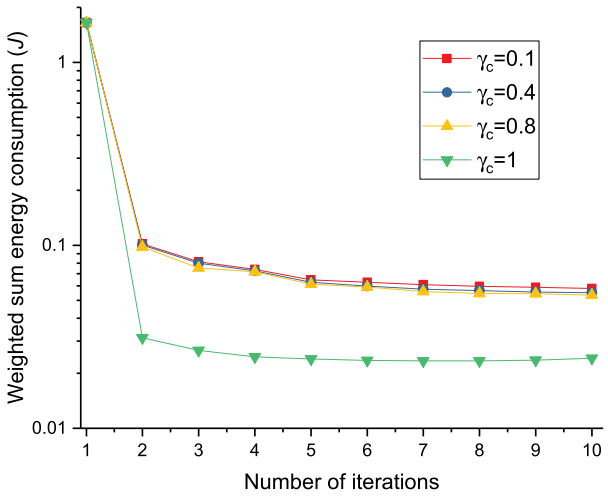

Fig. 7. Convergence of weighted sum energy consumption.

the figure, the proposed Algorithm 3 for solving the MOO problem converges quickly and only three or four iterations are required for the convergence. From the figure, a higher transmit power budget will lead to a higher objective function value as a larger transmit power budget will cause higher energy consumption in computation offloading. Meanwhile, the approximation value in MIMO radar beampattern design will also increase with transmit power budget, which is also revealed in Fig. 4.

Fig. 7 plots the weighted sum energy consumption versus the number of iterations to verify the convergence of the proposed algorithm under different values of weight coefficient γ_c. From the figure, the weighted sum energy consumption decreases quickly with the number of iterations and converges quickly with only 5 to 6 iterations. Moreover, the weighted sum energy consumption for computation offloading decreases as the value of γ_c increases because a larger γ_c indicates a higher priority on computation offloading energy saving. When $\gamma_c = 1$, only energy consumption is considered in the optimization objective and the resultant weighted sum energy consumption is the lowest. For $\gamma_c = 0.1$, 0.4, and 0.8, the performance gap is very small. By observing the objective function of computation offloading ($f(\mathbb{W}_c, \mathbb{W}_r, \mathbb{F}_l)$), communication precoding matrix is an important factor in determining the weighted sum energy consumption, as a smaller transmit power $\|\mathbf{W}_{c,k}\|_F^2$ and a larger r_k can lead to a smaller data offloading energy consumption of $E_{o,k}$. Meanwhile, as UT's radar receiver has complete knowledge of the transmitted communication symbols, the communication signal is also used for radar sensing in the proposed DFRC system. Thus, the covariance of UT k's transmit waveform, $\mathbf{R}_{\mathbf{X},k} = \mathbf{W}_{r,k}\mathbf{W}_{r,k}^H + \mathbf{W}_{c,k}\mathbf{W}_{c,k}^H$, as in equ. (3) is used in the multi-UT radar beampattern approximation problem. Since the desired MIMO radar beampattern, as stated in Section III.A, is designed with full transmission power budget. The multi-UT radar beampattern approximation objective in the MOO problem (Section III.C) will also try to use full transmit power to obtain a good MIMO radar beampattern for each UT. From the example in Fig. 4, given the transmit power budget,

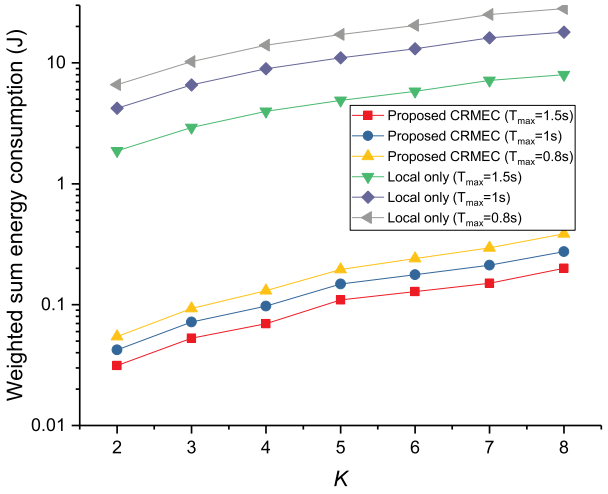

Fig. 8. Weighted sum energy consumption versus the number of UT.

the power allocation for radar sensing and communication is almost equally divided when $\gamma_c = 0.4$. Thus, the performance of computation offloading energy consumption is significantly affected by the radar optimization objective. Even for $\gamma_c = 0.8$, the multi-UT radar beampattern design will affect the optimization of communication precoding matrices and the resultant communication transmit power is high. Relevant result can also be seen in Fig. 3, where the performance difference is small for MSE of beampattern when $\gamma_c \neq 1$. Therefore, the difference of computation offloading energy consumption is not obvious for γ_c values of 0.1, 0.4 and 0.8.

Fig. 8 illustrates the weighted sum energy consumption versus the number of UTs under different maximum tolerable delay constraints. For performance comparison, the local only computing method (labelled as Local only) is considered, where the UT processes the radar data by using its local computing power. From the figure, the weighted sum energy consumption of the proposed CRMEC scheme and the local only method all increase as the number of UTs increases. Since the local computing power and efficiency are poor, the local

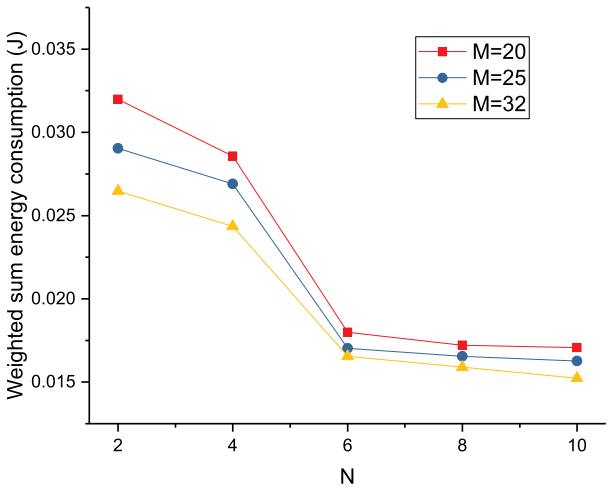

Fig. 9. Weighted sum energy consumption versus the UT and BS antenna number.

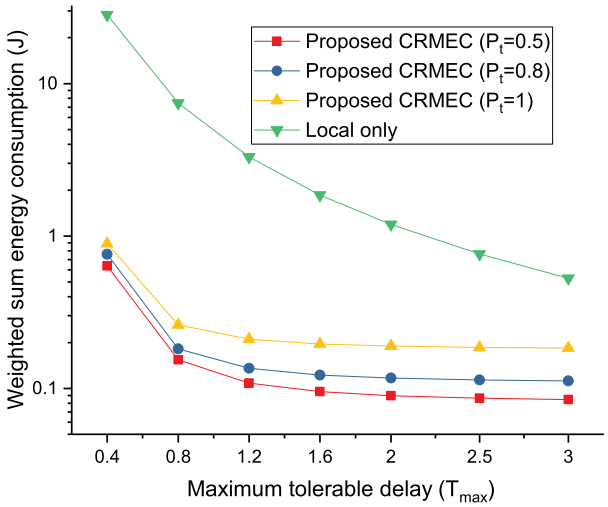

Fig. 11. Weighted sum energy consumption versus the maximum tolerable delay.

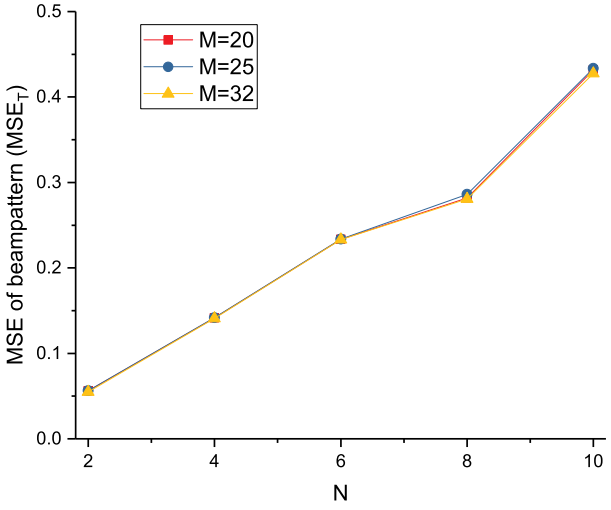

Fig. 10. MSE of beampattern versus the UT and BS antenna number.

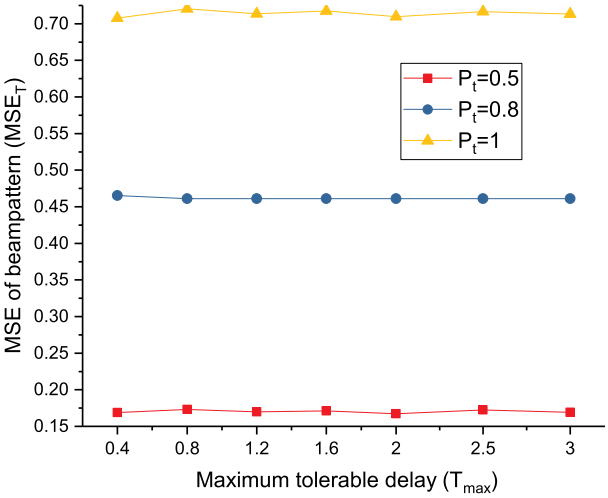

Fig. 12. MSE of beampattern versus the maximum tolerable delay.

only computing method has very high energy consumption. By using MIMO computation offloading and the strong computing power at the BS, the proposed CRMEC scheme has low energy consumption. In addition, we also consider the impact of maximum tolerable delay T_{max}. From the figure, the weighted sum energy consumption of the proposed CRMEC scheme and the local only computing method all increase as the delay constraint becomes more stringent because a shorter offloading delay constraint requires the UT to use more of its local computing resource and higher transmission power. Thus, the local computing delay and transmission delay can be reduced and the overall delay requirement is satisfied.

Fig. 9 plots the weighted sum energy consumption versus the UT antenna number for different BS antenna numbers. From the figure, the weighted sum energy consumption decreases quickly with the UT antenna number because a larger UT antenna number indicates that the UT can transmit more data streams and obtain higher transmission rate. Thus, the transmission delay and transmission energy consumption are both reduced. Accordingly, the UT has longer time to finish local computing and can use less local computation resource to reduce the local computation energy consumption. Moreover, the weighted sum energy consumption also decreases with the BS antenna number because increasing the number of receive antennas can improve the received signal quality and provide spatial multiplexing gain. To show the relationship between the MSE of beampattern and the UT antenna number, we use the total MSE of beampattern of all UTs and direction angles as follows

$$\mathrm{MSE}_T=\frac{1}{LK}\sum_{k=1}^{K}\sum_{l=1}^{L}\left|\eta_k P_{d,k}(\theta_l)-\mathbf{a}_k^H(\theta_l)\,\mathbf{R}_{\mathbf{X},k}\mathbf{a}_k(\theta_l)\right|^2. \quad (66)$$

Fig. 10 shows the $\mathrm{MSE_T}$ versus the UT antenna number under different BS antenna numbers. From Fig. 10, the $\mathrm{MSE_T}$ increases with the UT antenna number N because the obtained MIMO radar beampattern $\mathbf{R}_{\mathbf{X},k}$ is an $N\times N$ positive semidefinite matrix and a larger N indicates more elements in $\mathbf{R}_{\mathbf{X},k}$. Therefore, the accumulated error increases with N and the

$\mathrm{MSE_T}$ grows as well. Since the BS antenna number only has impact on its data reception, the impact of BS antenna number on $\mathrm{MSE_T}$ can be ignored and the $\mathrm{MSE_T}$ is almost unchanged for different M. According to Fig. 9 and Fig. 10, UT antenna number should be properly selected for the tradeoff between computation offloading energy consumption and the MIMO radar beampattern design.

Fig. 11 plots the weighted sum energy consumption versus the maximum tolerable delay T_{max} under different transmit power settings. From the figure, the weighted sum energy consumption of the proposed CRMEC scheme and local only computing method all decreases with the maximum tolerable delay because a less stringent delay constraint means that the UT can use less local computing resource on local computing at the cost of longer local computing delay, which can be seen from $f_{l,k}^{min}$ in equ. (62a). Due to the limited local computing ability, the local only computing method has the highest energy consumption. Moreover, the weighted sum energy consumption increases with the transmit power P_t, rather than converging to a similar value like [18] (Fig. 4) because the energy consumption is not the only objective in the designed CRMEC system and a higher transmit power for radar and communication leads to better radar performance. Therefore, a larger P_t has higher energy consumption, which is consistent with the power allocation result in Fig. 5.

Fig. 12 shows the impact of maximum tolerable delay T_{max} on the $\mathrm{MSE_T}$ under different transmit powers. From the figure, the $\mathrm{MSE_T}$ is not affected by the maximum tolerable delay T_{max} and stays stable w.r.t T_{max} because radar plays an important part in the optimization objective when $\gamma_c = 0.4$ and the available power is used to ensure the performance of MIMO radar. Therefore, T_{max} does not have influence on $\mathrm{MSE_T}$. In addition, higher transmit power P_t has larger $\mathrm{MSE_T}$ and similar explanation can be found in the illustration of Fig. 4.

VI. Conclusion

In this paper, we have proposed a communication, radar sensing, and MEC integrated architecture. We have formulated a MOO problem by jointly considering computation offloading and radar sensing. The tradeoff of these two objectives has been obtained by adjusting the weight coefficients. Block coordinate descent algorithm has been adopted to iteratively address the precoding design and computation resource allocation. We have used QTFP, first-order Taylor expansion, and WMMSE methods for problem transformation and solution derivation, which are efficient with low complexity. Simulation results revealed that the computation offloading energy consumption is low compare with the local only computing method and decreases when the energy consumption has high priority in the optimization objective. Meanwhile, the obtained radar beampattern can approximate the ideal radar beampattern very well.

Appendix A

From equ. (26), $\tilde{r}_k(\mathbf{W}_c, \gamma)$ is concave w.r.t γ when $\mathbb{W}_c$ is held fixed. By using the Sherman-Morrison formula, the optimal $\gamma_{k,l}$ can be found by setting $\partial \tilde{r}_k(\mathbf{W}_c, \gamma)/\partial \gamma_{k,l} = 0$, the derivative process can be formulated as equ. (67), as shown at the top of the next page.

Therefore, the optimal $\gamma_{k,l}$ is $\gamma_{k,l}^{opt} = \mathbf{w}_{c,k(l)}^H \mathbf{H}_k^H \mathbf{N}_k^{-1} \mathbf{H}_k \mathbf{w}_{c,k(l)}$. Substituting $\gamma_{k,l}^{opt}$ back in $\tilde{r}_k(\mathbf{W}_c, \gamma)$ in equ. (26) recovers the rate function $\tilde{r}_k$ in equ. (25), thereby the equivalence is established.

Appendix B

From equ. (42), $\tilde{r}_k(\mathbf{G}_k, \mathbb{W}_r, \mathbf{V}_k)$ is concave over $\mathbf{G}_k$ with fixed $\mathbf{W}_r$. Hence, the optimal $\mathbf{G}_k$ is obtained by setting $\partial \tilde{r}_k(\mathbf{G}_k, \mathbb{W}_r, \mathbf{V}_k)/\partial \mathbf{G}_k = \mathbf{0}$ and is formulated as

$$\frac{\partial \tilde{r}_k(\mathbf{G}_k, \mathbb{W}_r, \mathbf{V}_k)}{\partial \mathbf{G}_k} = (\mathbf{G}_k)^{-T} - (\mathbf{E}_k)^T. \tag{68}$$

Accordingly, we have $\mathbf{G}_k^{opt} = \mathbf{E}_k$. By substituting the optimal $\mathbf{V}_k$ and $\mathbf{G}_k$ in equ. (41), $\tilde{r}_k(\mathbf{G}_k, \mathbb{W}_r, \mathbf{V}_k)$ can be written as equ. (69), as shown at the top of the next page.

In equ. (69), Sherman-Morrison formula is applied in (a), and the property of $\det(\mathbf{I} + \mathbf{A}_1\mathbf{A}_2) = \det(\mathbf{I} + \mathbf{A}_2\mathbf{A}_1)$ is used in (b).

Appendix C

Given δ and μ, the optimal radar precoding matrix $\mathbf{W}_{r,k}^{opt}$ can be obtained by setting $\partial L/\partial \mathbf{W}_{r,k}$=$\mathbf{0}$. According to the expression of $L(\mathbb{W}_r, \mathbf{t}, \delta, \mu)$ in equ. (53), the first-order derivative of L w.r.t $\mathbf{W}_{r,k}$ can be given by equ. (70), as shown at the top of the next page.

In equ. (70), $\chi_k = \gamma_c \gamma_k^c \beta_k B_k \|\mathbf{W}_{c,k}\|_F^2 t_k^2 + \mu_k$, $\mathbf{P}_k = \mathbf{G}_k^H + \mathbf{G}_k$, and $\mathbf{G}_{r,k}$ is given by [47]

$$\mathbf{G}_{r,k} = (1/2)\left(\nabla g_r\left(\mathbf{W}_{r,k}^n\right) + \left(\nabla g_r\left(\mathbf{W}_{r,k}^n\right)\right)^H\right). \tag{71}$$

Then, we have

$$\chi_k \mathbf{H}_k^H \mathbf{V}_k \mathbf{V}_k^H \mathbf{H}_k \mathbf{W}_{r,k} \mathbf{P}_k + 2\delta_k \mathbf{W}_{r,k} = -\gamma_r \gamma_k^r \mathbf{G}_{r,k}, \tag{72}$$

which can be further written as

$$\left[\chi_k \mathbf{H}_k^H \mathbf{V}_k \mathbf{V}_k^H \mathbf{H}_k 2\delta_k \mathbf{I}_N\right] \begin{bmatrix} \mathbf{W}_{r,k}\mathbf{P}_k \\ \mathbf{W}_{r,k} \end{bmatrix} = -\gamma_r \gamma_k^r \mathbf{G}_{r,k}. \tag{73}$$

By using Moore-Penrose inverse, equ. (73) can be reformulated by

$$\begin{bmatrix} \mathbf{W}_{r,k}\mathbf{P}_k \\ \mathbf{W}_{r,k} \end{bmatrix} = \left(\left[\chi_k \mathbf{H}_k^H \mathbf{V}_k \mathbf{V}_k^H \mathbf{H}_k 2\delta_k \mathbf{I}_N\right]\right)^{\dagger} \left(-\gamma_r \gamma_k^r \mathbf{G}_{r,k}\right). \tag{74}$$

Therefore, the optimal $\mathbf{W}_{r,k}^{opt}$ can be derived according to the right hand side of equ. (74).

Appendix D

To prove the convergence of Algorithm 3, we need to show that the objective function value of the MOO problem (22) is nonincreasing when the variable sets $(\mathbb{W}_r, \mathbb{W}_c, \mathbb{F}_l, \mathbb{F}_e)$ are updated after each iteration. Define

$$V(\mathbb{W}_c, \mathbb{W}_r, \mathbb{F}_l, \mathbb{F}_e) = \gamma_c f(\mathbb{W}_c, \mathbb{W}_r, \mathbb{F}_l) + \gamma_r g(\mathbb{W}_c, \mathbb{W}_r) \tag{75}$$

as the objective function value of the MOO problem (22). Then, according to Algorithm 3, we have

$$V_{obj}^{(n-1)} = V\left(\mathbb{W}_c^{(n-1)}, \mathbb{W}_r^{(n-1)}, \mathbb{F}_l^{(n-1)}, \mathbb{F}_e^{(n-1)}\right)$$

$$\begin{aligned}\frac{\partial \tilde{r}_k\left(\mathbf{W}_c,\gamma\right)}{\partial \gamma_{k,l}} &= \frac{1}{1+\gamma_{k,l}} - 1 + \mathbf{w}_{c,k(l)}^H \mathbf{H}_k^H \mathbf{U}_{k,l}^{-1} \mathbf{H}_k \mathbf{w}_{c,k(l)} \\ &= \frac{-\gamma_{k,l}}{1+\gamma_{k,l}} + \mathbf{w}_{c,k(l)}^H \mathbf{H}_k^H \left(\mathbf{H}_k \mathbf{w}_{c,k(l)} \mathbf{w}_{c,k(l)}^H \mathbf{H}_k^H + \mathbf{N}_k\right)^{-1} \mathbf{H}_k \mathbf{w}_{c,k(l)} \\ &= \frac{-\gamma_{k,l}}{1+\gamma_{k,l}} + \mathbf{w}_{c,k(l)}^H \mathbf{H}_k^H \mathbf{N}_k^{-1} \mathbf{H}_k \mathbf{w}_{c,k(l)} \\ &\quad - \frac{\mathbf{w}_{c,k(l)}^H \mathbf{H}_k^H \mathbf{N}_k^{-1} \mathbf{H}_k \mathbf{w}_{c,k(l)} \mathbf{w}_{c,k(l)}^H \mathbf{H}_k^H \mathbf{N}_k^{-1} \mathbf{H}_k \mathbf{w}_{c,k(l)}}{1 + \mathbf{w}_{c,k(l)}^H \mathbf{H}_k^H \mathbf{N}_k^{-1} \mathbf{H}_k \mathbf{w}_{c,k(l)}} \\ &= \frac{-\gamma_{k,l}}{1+\gamma_{k,l}} + \frac{\mathbf{w}_{c,k(l)}^H \mathbf{H}_k^H \mathbf{N}_k^{-1} \mathbf{H}_k \mathbf{w}_{c,k(l)}}{1 + \mathbf{w}_{c,k(l)}^H \mathbf{H}_k^H \mathbf{N}_k^{-1} \mathbf{H}_k \mathbf{w}_{c,k(l)}}. \end{aligned} \tag{67}$$

$$\begin{aligned}\tilde{r}_k\left(\mathbf{G}_k,\mathbf{W}_r,\mathbf{V}_k\right) &= \log\det\left(\mathbf{G}_k^{opt}\right) - \mathrm{Tr}\left(\mathbf{G}_k^{opt}\mathbf{E}_k\right) + d \\ &= \log\det\left(\left(\mathbf{E}_k^*\right)^{-1}\right) - \mathrm{Tr}\left(\mathbf{I}_d\right) + d \\ &= \log\det\left(\left(\mathbf{I}_d - \mathbf{W}_{c,k}^H \mathbf{H}_k^H \mathbf{\Pi}_k^{-1} \mathbf{H}_k \mathbf{W}_{c,k}\right)^{-1}\right) \\ &\overset{(a)}{=} \log\det\left(\mathbf{I}_d^{-1} + \mathbf{I}_d^{-1} \mathbf{W}_{c,k}^H \mathbf{H}_k^H \left(\mathbf{\Pi}_k - \mathbf{H}_k \mathbf{W}_{c,k} \mathbf{I}_d^{-1} \mathbf{W}_{c,k}^H \mathbf{H}_k^H\right)^{-1} \mathbf{H}_k \mathbf{W}_{c,k}\right) \\ &= \log\det\left(\mathbf{I}_d + \mathbf{W}_{c,k}^H \mathbf{H}_k^H \mathbf{N}_k^{-1} \mathbf{H}_k \mathbf{W}_{c,k}\right) \\ &\overset{(b)}{=} \log\det\left(\mathbf{I}_d + \mathbf{H}_k \mathbf{W}_{c,k} \mathbf{W}_{c,k}^H \mathbf{H}_k^H \mathbf{N}_k^{-1}\right) \\ &= r_k. \end{aligned} \tag{69}$$

$$\begin{aligned}\frac{\partial L}{\partial \mathbf{W}_{r,k}} &= -\left(\gamma_c \gamma_k^c \beta_k B_k \left\|\mathbf{W}_{c,k}\right\|_F^2 t_k^2 + \mu_k\right) \frac{\partial \tilde{r}_k}{\partial \mathbf{W}_{r,k}} + \gamma_r \gamma_k^r \frac{\partial g_r\left(\mathbf{W}_{r,k}, \mathbf{W}_{r,k}^n\right)}{\partial \mathbf{W}_{r,k}} \\ &\quad + \delta_k \frac{\partial \left\|\mathbf{W}_{c,k}\right\|_F^2}{\partial \mathbf{W}_{r,k}} \\ &= \chi_k \mathbf{H}_k^H \mathbf{V}_k \mathbf{V}_k^H \mathbf{H}_k \mathbf{W}_{r,k} \mathbf{P}_k + \gamma_r \gamma_k^r \mathbf{G}_{r,k} + 2\delta_k \mathbf{W}_{r,k}, \end{aligned} \tag{70}$$

$$\begin{aligned}&\overset{(\mathrm{I})}{\geq} V\left(\mathbb{W}_c^{(n)}, \mathbb{W}_r^{(n-1)}, \mathbb{F}_l^{(n-1)}, \mathbb{F}_e^{(n-1)}\right) \\ &\overset{(\mathrm{II})}{\geq} V\left(\mathbb{W}_c^{(n)}, \mathbb{W}_r^{(n)}, \mathbb{F}_l^{(n-1)}, \mathbb{F}_e^{(n)}\right) \\ &\overset{(\mathrm{III})}{\geq} V\left(\mathbb{W}_c^{(n)}, \mathbb{W}_r^{(n)}, \mathbb{F}_l^{(n)}, \mathbb{F}_e^{(n)}\right) \\ &\overset{(\mathrm{IV})}{=} V_{obj}^{(n)}. \end{aligned} \tag{76}$$

Inequality (I) is obtained from that $\mathbb{W}_c^{(n)}$ is one suboptimal precoding design of problem (23) with fixed radar precoding $\mathbb{W}_r^{(n-1)}$, local and edge computation resource allocation $\mathbb{F}_l^{(n-1)}$ and $\mathbb{F}_e^{(n-1)}$. Inequality (II) is derived from that $\mathbb{W}_r^{(n)}$ and $\mathbb{F}_e^{(n)}$ are the optimal radar precoding design and edge computation resource allocation of problem (36) with fixed communication precoding design $\mathbb{W}_c^{(n)}$ and local computation resource allocation $\mathbb{F}_l^{(n-1)}$. Inequality (III) follows from that $\mathbb{F}_l^{(n)}$ is the optimal solution of problem (62) with fixed communication precoding design $\mathbb{W}_c^{(n)}$, radar precoding design $\mathbb{W}_r^{(n)}$, and edge computation resource allocation $\mathbb{F}_e^{(n)}$. According to the last equation (IV), we can know that the objective function value of the MOO problem (22) is nonincreasing after optimizing the variables in each iteration, and the convergence of Algorithm 3 is proved.

ACKNOWLEDGMENT

The authors would like to thank Prof. Gang Xu of the National Mobile Communications Research Laboratory, Southeast University, for his kind help.

REFERENCES

[1] Q. Huang, H. Chen, and Q. Zhang, "Joint design of sensing and communication systems for smart homes," *IEEE Netw.*, vol. 34, no. 6, pp. 191–197, Nov. 2020.

[2] D. Ma, N. Shlezinger, T. Huang, Y. Liu, and Y. C. Eldar, "Joint radar-communication strategies for autonomous vehicles: Combining two key automotive technologies," *IEEE Signal Process. Mag.*, vol. 37, no. 4, pp. 85–97, Jul. 2020.

[3] R. W. Heath, Jr., "Communications and sensing: An opportunity for automotive systems," *IEEE Signal Process. Mag.*, vol. 37, no. 4, pp. 3–13, Jul. 2020.

[4] F. Liu, C. Masouros, A. Li, H. Sun, and L. Hanzo, "MU-MIMO communications with MIMO radar: From co-existence to joint transmission," *IEEE Trans. Wireless Commun.*, vol. 17, no. 4, pp. 2755–2770, Apr. 2018.

[5] F. Liu, C. Masouros, A. P. Petropulu, H. Griffiths, and L. Hanzo, "Joint radar and communication design: Applications, state-of-the-art, and the road ahead," *IEEE Trans. Commun.*, vol. 68, no. 6, pp. 3834–3862, Jun. 2020.

[6] N. C. Luong, X. Lu, D. T. Hoang, D. Niyato, and D. I. Kim, "Radio resource management in joint radar and communication: A comprehensive survey," *IEEE Commun. Surveys Tuts.*, vol. 23, no. 2, pp. 780–814, 2nd Quart., 2021.

[7] M. Rihan and L. Huang, "Optimum co-design of spectrum sharing between MIMO radar and MIMO communication systems: An interference alignment approach," *IEEE Trans. Veh. Technol.*, vol. 67, no. 12, pp. 11667–11680, Dec. 2018.

[8] S. Sodagari, A. Khawar, T. C. Clancy, and R. McGwier, "A projection based approach for radar and telecommunication systems coexistence," in *Proc. IEEE Global Commun. Conf. (GLOBECOM)*, Anaheim, CA, USA, Dec. 2012, pp. 5010–5014.

[9] F. Liu, C. Masouros, A. Li, T. Ratnarajah, and J. Zhou, "MIMO radar and cellular coexistence: A power-efficient approach enabled by interference exploitation," *IEEE Trans. Signal Process.*, vol. 66, no. 14, pp. 3681–3695, Jul. 2018.

[10] A. Hassanien, M. G. Amin, E. Aboutanios, and B. Himed, "Dual-function radar communication systems: A solution to the spectrum congestion problem," *IEEE Signal Process. Mag.*, vol. 36, no. 5, pp. 115–126, Sep. 2019.

[11] X. Liu, T. Huang, N. Shlezinger, Y. Liu, J. Zhou, and Y. C. Eldar, "Joint transmit beamforming for multiuser MIMO communications and MIMO radar," *IEEE Trans. Signal Process.*, vol. 68, pp. 3929–3944, 2020.

[12] C. B. Barneto, S. D. Liyanaarachchi, T. Riihonen, L. Anttila, and M. Valkama, "Multibeam design for joint communication and sensing in 5G new radio networks," in *Proc. IEEE Int. Conf. Commun. (ICC)*, Dublin, Ireland, Jun. 2020, pp. 1–6.

[13] S. Buzzi, C. D'Andrea, and M. Lops, "Transmit power allocation for joint communication and sensing through massive MIMO arrays," in *Proc. 24th Int. ITG Workshop Smart Antennas*, Hamburg, Germany, Feb. 2020, pp. 1–6.

[14] A. Farina, "Introduction to radar signal and data processing: The opportunity," SELEX Sistemi Integrati, Rome, Italy, Tech. Rep., 2006.

[15] A. Davoli, G. Guerzoni, and G. M. Vitetta, "Machine learning and deep learning techniques for colocated MIMO radars: A tutorial overview," *IEEE Access*, vol. 9, pp. 33704–33755, 2021.

[16] Y. Xia *et al.*, "Learning-based extended object tracking using hierarchical truncation measurement model with automotive radar," *IEEE J. Sel. Topics Signal Process.*, vol. 15, no. 4, pp. 1013–1029, Jun. 2021.

[17] Y. Mao, C. You, J. Zhang, K. Huang, and K. B. Letaief, "A survey on mobile edge computing: The communication perspective," *IEEE Commun. Surveys Tuts.*, vol. 19, no. 4, pp. 2322–2358, Aug. 2017.

[18] C. Ding, J.-B. Wang, H. Zhang, M. Lin, and J. Wang, "Joint MU-MIMO precoding and resource allocation for mobile-edge computing," *IEEE Trans. Wireless Commun.*, vol. 20, no. 3, pp. 1639–1654, Mar. 2021.

[19] S. Guangmin, L. Guosui, and G. Hong, "Signal analysis and processing for random binary phase coded pulse radar," *J. Syst. Eng. Electron.*, vol. 15, no. 4, pp. 520–524, Dec. 2004.

[20] D. V. Sarwate and M. B. Pursley, "Crosscorrelation properties of pseudorandom and related sequences," *Proc. IEEE*, vol. 68, no. 5, pp. 593–619, May 1980.

[21] D. R. Fuhrmann and G. S. Antonio, "Transmit beamforming for MIMO radar systems using signal cross-correlation," *IEEE Trans. Aerosp. Electron. Syst.*, vol. 44, no. 1, pp. 171–186, Jan. 2008.

[22] M.-A. Govoni, *Linear Frequency Modulation of Stochastic Radar Waveform*. Hoboken, NJ, USA: Stevens Inst. Technol., 2011.

[23] D. C. Bell and R. M. Narayanan, "Theoretical aspects of radar imaging using stochastic waveforms," *IEEE Trans. Signal Process.*, vol. 49, no. 2, pp. 394–400, Feb. 2001.

[24] D. Li, X. Li, Y. Qin, Y. Cheng, and H. Wang, "Radar coincidence imaging: An instantaneous imaging technique with stochastic signals," *IEEE Trans. Geosci. Remote Sens.*, vol. 52, no. 4, pp. 2261–2277, Apr. 2014.

[25] D. Wu, M. M. Omwenga, Y. Liang, L. Yang, D. Huston, and T. Xia, "Edge computing enabled cognitive portable ground penetrating radar," in *Proc. 12th EAI Int. Conf. Mobile Multimedia Commun.* Weihai, China: European Alliance for Innovation, Jun. 2019, p. 127.

[26] A. Farina and F. Studer, "Radar data processing. Volume 2-advanced topics and applications," *NASA STI/Recon Tech. Rep. A*, vol. 86, p. 38224, Feb. 1986.

[27] P. Wang, Z. Zheng, B. Di, and L. Song, "HetMEC: Latency-optimal task assignment and resource allocation for heterogeneous multi-layer mobile edge computing," *IEEE Trans. Wireless Commun.*, vol. 18, no. 10, pp. 4942–4956, Oct. 2019.

[28] J.-B. Wang, J. Zhang, C. Ding, H. Zhang, M. Lin, and J. Wang, "Joint optimization of transmission bandwidth allocation and data compression for mobile-edge computing systems," *IEEE Commun. Lett.*, vol. 24, no. 10, pp. 2245–2249, Oct. 2020.

[29] M. Sheng, Y. Wang, X. Wang, and J. Li, "Energy-efficient multiuser partial computation offloading with collaboration of terminals, radio access network, and edge server," *IEEE Trans. Commun.*, vol. 68, no. 3, pp. 1524–1537, Mar. 2020.

[30] T. Q. Dinh, J. Tang, Q. D. La, and T. Q. S. Quek, "Offloading in mobile edge computing: Task allocation and computational frequency scaling," *IEEE Trans. Commun.*, vol. 65, no. 8, pp. 3571–3584, Aug. 2017.

[31] X. Chen, L. Jiao, W. Li, and X. Fu, "Efficient multi-user computation offloading for mobile-edge cloud computing," *IEEE/ACM Trans. Netw.*, vol. 24, no. 5, pp. 2795–2808, Oct. 2016.

[32] C. Wang, C. Liang, F. R. Yu, Q. Chen, and L. Tang, "Computation offloading and resource allocation in wireless cellular networks with mobile edge computing," *IEEE Trans. Wireless Commun.*, vol. 16, no. 8, pp. 4924–4938, Aug. 2017.

[33] A. Khawar, A. Abdelhadi, and C. Clancy, "Target detection performance of spectrum sharing MIMO radars," *IEEE Sensors J.*, vol. 15, no. 9, pp. 4928–4940, Sep. 2015.

[34] J. Li and P. Stoica, *MIMO Radar Signal Processing*. Hoboken, NJ, USA: Wiley, 2008.

[35] B. Li and A. P. Petropulu, "Joint transmit designs for coexistence of MIMO wireless communications and sparse sensing radars in clutter," *IEEE Trans. Aerosp. Electron. Syst.*, vol. 53, no. 6, pp. 2846–2864, Dec. 2017.

[36] M. A. Richards, *Fundamentals of Radar Signal Processing*. New York, NY, USA: McGraw-Hill, 2014.

[37] N. Su, F. Liu, and C. Masouros, "Secure radar-communication systems with malicious targets: Integrating radar, communications and jamming functionalities," *IEEE Trans. Wireless Commun.*, vol. 20, no. 1, pp. 83–95, Jan. 2021.

[38] P. Stoica, J. Li, and Y. Xie, "On probing signal design for MIMO radar," *IEEE Trans. Signal Process.*, vol. 55, no. 8, pp. 4151–4161, Aug. 2007.

[39] W. Dinkelbach, "On nonlinear fractional programming," *Manage. Sci.*, vol. 13, no. 7, pp. 492–498, Mar. 1967.

[40] Y. Jong, "Practical global optimization algorithm for the sum-of-ratios problem," 2012, *arXiv:1207.1153*.

[41] S. Schaible and J. Shi, "Fractional programming: The sum-of-ratios case," *Optim. Methods Softw.*, vol. 18, no. 2, pp. 219–229, Apr. 2003.

[42] K. Shen and W. Yu, "Fractional programming for communication systems—Part I: Power control and beamforming," *IEEE Trans. Signal Process.*, vol. 66, no. 10, pp. 2616–2630, May 2018.

[43] Q. Shi, M. Razaviyayn, Z.-Q. Luo, and C. He, "An iteratively weighted MMSE approach to distributed sum-utility maximization for a MIMO interfering broadcast channel," *IEEE Trans. Signal Process.*, vol. 59, no. 9, pp. 4331–4340, Sep. 2011.

[44] S. P. Boyd and L. Vandenberghe, *Convex Optimization*. Cambridge, U.K.: Cambridge Univ. Press, 2014.

[45] D. P. Bertsekas, *Convex Optimization Theory*. Belmon, MA, USA: Athena Scientific, 2009.

[46] *Physical Layer Aspects for Evolved Universal Terrestrial Radio Access (UTRA) (Release 7)*, 3GPP, document TR 25.814, 2006.

[47] X. Zhang, *Matrix Analysis and Applications*. Cambridge, U.K.: Cambridge Univ. Press, 2017.

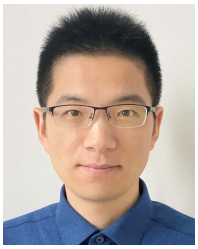

Changfeng Ding (Graduate Student Member, IEEE) received the B.S. degree in communication engineering from Nanjing Tech University, Nanjing, China, in 2015, and the M.S. degree in information and communication engineering from Southwest Jiaotong University, Chengdu, China, in 2018. He is currently pursuing the Ph.D. degree with the National Mobile Communications Research Laboratory, Southeast University, Nanjing. His current research interests include applications of MIMO communication, mobile edge computing, and satellite communication.

Jun-Bo Wang (Member, IEEE) received the B.S. degree in computer science from the Hefei University of Technology, Hefei, China, in 2003, and the Ph.D. degree in communications engineering from Southeast University, Nanjing, China, in 2008. From October 2008 to August 2013, he was with the Nanjing University of Aeronautics and Astronautics, China. From February 2011 to February 2013, he was a Post-Doctoral Fellow with the National Laboratory for Information Science and Technology, Tsinghua University, China. Since August 2013, he has been an Associate Professor with the National Mobile Communications Research Laboratory, Southeast University. From October 2016 to September 2018, he held the European Commission Marie Curie Fellowship and was a Research Fellow with the University of Kent, U.K. His current research interests include cloud radio access networks, mmWave communications, and wireless optical communications.

Hua Zhang (Member, IEEE) received the B.S. and M.S. degrees from the Department of Radio Engineering, Southeast University, Nanjing, China, in 1998 and 2001, respectively, and the Ph.D. degree from the School of Electrical and Computer Engineering, Georgia Institute of Technology, in 2004. From 2001 to 2004, he was a Graduate Research Assistant with the Georgia Institute of Technology. From 2004 to 2005, he worked as a Senior System Engineer with Skyworks Solutions Inc., Irvine, CA, USA. From 2005 to 2006, he worked as a Staff Engineer with MaxLinear Inc., Carlsbad, CA, USA. Since August 2006, he has been an Associate Professor with the School of Information Science and Engineering, Southeast University. His current research interests include massive MIMO, software-defined radio, and cooperative communications. He received the Best Paper Award of IEEE MAPE in 2013 and IEEE GLOBECOM in 2014.

Min Lin (Member, IEEE) received the B.S. degree from the National University of Defense Technology, Changsha, China, in 1993, the M.S. degree from the Nanjing Institute of Communication Engineering, Nanjing, China, in 2000, and the Ph.D. degree from Southeast University, Nanjing, in 2008, all in electrical engineering. From April 2015 to October 2015, he has visited the University of California, Irvine, as a Senior Research Fellow. He is currently a Professor and a Supervisor of Ph.D. and graduate students with the Nanjing University of Posts and Telecommunications, Nanjing. He has authored or coauthored over 130 articles. His current research interests include wireless communications and array signal processing. He has served as the Track Chair for Satellite and Space Communications (SSC) of IEEE ICC 2019 and GLOBECOM 2021, and a TPC member for many IEEE sponsored conferences.

Geoffrey Ye Li (Fellow, IEEE) is currently the Chair Professor with Imperial College London, U.K. Before moving to Imperial College London in 2020, he was a Professor with the Georgia Institute of Technology, USA, for 20 years; and a Principal Technical Staff Member with AT&T Labs—Research, NJ, USA, for five years. His general research interests include statistical signal processing and machine learning for wireless communications. In the related areas, he has published over 600 journal and conference articles in addition to over 40 granted patents and several books. His publications have been cited over 50 000 times with an H-index over 100 and he has been recognized as a Highly Cited Researcher, by Thomson Reuters, almost every year. He was awarded an IEEE Fellow and an IET Fellow for his contributions to signal processing for wireless communications. He won several prestigious awards from the IEEE Signal Processing Society (the Donald G. Fink Overview Paper Award in 2017), the IEEE Vehicular Technology Society (the James Evans Avant Garde Award in 2013 and the Jack Neubauer Memorial Award in 2014), and the IEEE Communications Society (the Stephen O. Rice Prize Paper Award in 2013, the Award for Advances in Communication in 2017, and the Edwin Howard Armstrong Achievement Award in 2019). He also received the 2015 Distinguished ECE Faculty Achievement Award from Georgia Tech. He has been involved in editorial activities for over 20 technical journals, including the founding Editor-in-Chief of IEEE JOURNAL ON SELECTED AREAS IN COMMUNICATIONS (IEEE JSAC) Special Series on ML in Communications and Networking. He has organized and chaired many international conferences, including the Technical Program Vice-Chair of the IEEE ICC03, and the General Co-Chair of IEEE GlobalSIP14, IEEE VTC19 (Fall), and IEEE SPAWC20.